Modeled and observed impacts of the 1997-1998 El Niño on nitrate and new production in the equatorial Pacific

Marie-Hélène Radenac, Christophe E. Menkès, Jérôme Vialard, Cyril Moulin, Yves Dandonneau, Thierry Delcroix, Cecile Dupouy, A. Stoens, Pierre-Yves Deschamps

▶ **To cite this version:**

Marie-Hélène Radenac, Christophe E. Menkès, Jérôme Vialard, Cyril Moulin, Yves Dandonneau, et al.. Modeled and observed impacts of the 1997-1998 El Niño on nitrate and new production in the equatorial Pacific. Journal of Geophysical Research, 2001, 106 (C11), pp.26879-26898. 10.1029/2000JC000546 . hal-00153957

HAL Id: hal-00153957
https://hal.science/hal-00153957v1

Submitted on 20 May 2021

HAL is a multi-disciplinary open access archive for the deposit and dissemination of scientific research documents, whether they are published or not. The documents may come from teaching and research institutions in France or abroad, or from public or private research centers.

L'archive ouverte pluridisciplinaire **HAL**, est destinée au dépôt et à la diffusion de documents scientifiques de niveau recherche, publiés ou non, émanant des établissements d'enseignement et de recherche français ou étrangers, des laboratoires publics ou privés.

JOURNAL OF GEOPHYSICAL RESEARCH, VOL. 106, NO. C11, PAGES 26,879-26,898, NOVEMBER 15, 2001

Modeled and observed impacts of the 1997-1998 El Niño on nitrate and new production in the equatorial Pacific

M.-H. Radenac,[1,2] C. Menkes,[1] J. Vialard,[1] C. Moulin,[3] Y. Dandonneau,[1]
T. Delcroix,[4] C. Dupouy,[1] A. Stoens,[3] and P.-Y. Deschamps[5]

Abstract. The impact of the strong 1997-1998 El Niño event on nitrate distribution and new production in the equatorial Pacific is investigated, using a combination of satellite and in situ observations, and an ocean circulation-biogeochemical model. The general circulation model is forced with realistic wind stresses deduced from ERS-1 and ERS-2 scatterometers over the 1993-1998 period. Its outputs are used to drive a biogeochemical model where biology is parameterized as a nitrate sink. We first show that the models capture the essential circulation and biogeochemical equatorial features along with their temporal evolution during the 1997-1998 event, although the modeled variability seems underestimated. In particular, the model fails to reproduce unusual bloom conditions. This is attributed to the simplicity of the biological model. An analysis of the physical mechanisms responsible for the dramatic decrease of the biological equatorial production during El Niño is then proposed. During the growth phase (November 1996 through June 1997), nitrate-poor waters of the western Pacific are advected eastward, and the vertical supply of nitrate is reduced due to nitracline deepening. These processes result in the invasion of the equatorial Pacific by nitrate-poor waters during the mature phase (November 1997 through January 1998). At that time, the central Pacific is nitrate limited and experiences warm pool oligotrophic conditions. As a result, the modeled new production over the equatorial Pacific drops by 40% compared to the mean 1993-1996 values. Then, while El Niño conditions are still present at the surface, the nitracline shallows over most of the basin in early 1998. Therefore the strengthening of the trade winds in May 1998 efficiently switches on the nitrate vertical supply over a large part of the equatorial Pacific, leading to a rapid return of high biological production conditions. Strong La Niña conditions then develop, resulting in a biologically rich tongue extending as far west as 160°E for several months.

1. Introduction

During non-El Niño years, the equatorial Pacific is characterized by west-east gradients of heat, nutrients, primary production, and plankton biomass and structure, between the warm pool and the upwelled waters. The transition between the fresh and oligotrophic warm pool and the salty and productive cold tongue is not smooth, but marked by a sharp salinity front [*Kuroda and McPhaden*, 1993; *Eldin et al.*, 1997], while the sea surface temperature (SST) gradient decreases more gradually. This front is a region of water convergence [*Picaut et al.*, 1996; *Vialard and Delecluse*, 1998] where the mean zonal currents approach zero [*Reverdin et al.*, 1994]. Moreover, observations and physical-biogeochemical models have shown that the salinity front is also the site of a discontinuity of nutrients and chlorophyll [*Eldin et al.*, 1997; *Stoens et al.*, 1999], zooplankton biomass [*Le Borgne and Rodier*, 1997], and partial pressure of CO_2 [*Inoue et al.*, 1996; *Boutin et al.*, 1999].

West of the front, the fresh warm pool is oligotrophic, featuring nitrate- and chlorophyll-depleted surface waters with near-zero new production. The nitracline depth is closely associated with the thermocline depth (below 100 m in the warm pool). A subsurface chlorophyll maximum and a weak new production maximum are located in the vicinity of the nitracline [*Navarette*, 1998]. Estimates of new production in oligotrophic regions of the equatorial Pacific vary from 0.5 mmol N m^{-2} d^{-1} [*Peña et al.*, 1994] to 1.2 mmol N m^{-2} d^{-1} [*Navarette*, 1998]. The ocean circulation variability is characterized by intraseasonal scales with features such as Kelvin waves forced by intraseasonal westerlies [*Kessler et al.*, 1995] and by interannual scales related to the large-scale El Niño-Southern Oscillation (ENSO) disruption [*Kessler et al.*, 1996].

East of the front, in the cold tongue, the surface layer is quasi-homogeneous with higher salinity, nitrate, and chlorophyll concentrations [*Wyrtki and Kilonsky*, 1984; *Barber and Kogelschatz*, 1990]. Here, surface chlorophyll concentrations are higher than in oligotrophic regions. The chlorophyll vertical profile shows a smooth maximum

[1]Laboratoire d'Océanographie Dynamique et de Climatologie, CNRS-IRD-Université Paris VI, Paris, France.
[2]Now at Laboratoire d'Études en Géophysique et Océanographie Spatiales, CNRS-CNES-IRD-Université Paul Sabatier, Toulouse, France.
[3]Laboratoire des Sciences du Climat et de l'Environnement, CEA-CNRS, Gif sur Yvette, France.
[4]Institut de Recherche pour le Développement, Nouméa, New Caledonia.
[5]Laboratoire d'Optique Atmosphérique, Lille, France.

Copyright 2001 by the American Geophysical Union.

Paper number 2000JC000546.
0148-0227/01/2000JC000546$09.00

between 40 and 70 m depth. The new production decreases downward from a near-surface maximum [*Navarette*, 1998]. The cold tongue is referred to as a "high-nutrient-low-chlorophyll" (HNLC) region [*Minas et al.*, 1986] where the phytoplankton biomass is low relative to available nitrate concentrations in the euphotic layer. This paradoxical lack of productivity despite persistent surface nitrate is explained by an efficient grazing by small phytoplankton [*Landry et al.*, 1997] and by micronutrients limitation (i.e., iron) [*Gordon et al.*, 1997]. Scales of variability include peaks of intraseasonal activities (tropical instability waves [*Baturin and Niiler*, 1997; *Vialard et al.*, 2001] and long equatorial Kelvin waves forced in the western and central Pacific [*Kessler et al.*, 1995; *Boulanger and Menkes*, 1999]), as well as clear semiannual, annual [*Yu and McPhaden*, 1999], and ENSO signals. The very active circulation dynamics of the region characterize the ecosystem responses. Thus the estimates of integrated new production in the central Pacific span a wide range (0.7 mmol N m^{-2} d^{-1} [*McCarthy et al.*, 1996] to 4.3 mmol N m^{-2} d^{-1} [*Carr et al.*, 1995]).

The modifications of the mean state of the oceanic circulation during El Niño events have been largely documented in recent years because of the improvement of observing systems and models during the Tropical Ocean Global Atmosphere (TOGA; 1985-1994) program [*McPhaden et al.*, 1998]. Observations include many research cruises (among them, repeated cruises along 165°E [*Delcroix et al.*, 1992] and along 110°W [*McPhaden and Hayes*, 1990]), the Tropical Atmosphere Ocean (TAO) mooring array [*Hayes et al.*, 1991; *McPhaden et al.*, 1998], and remotely sensed signals such as altimetry [*Fu et al.*, 1994]. Many ocean circulation models with growing levels of complexity have contributed to a better understanding of the ENSO theory. *Neelin et al.* [1998] reviewed such progress during the TOGA decade.

Description and simulation of ENSO-related disruption of nutrients and biology are less numerous because of the scarcity of in situ and remotely sensed data, and because the modeling of the three-dimensional (3-D) biogeochemical conditions inevitably lags the development of ocean circulation models. Nevertheless, recent studies show ENSO modifying the east-west asymmetry of nutrients and biology of the Pacific equatorial basin as it does for thermohaline features. These conclusions are derived from studies using merchants ships [*Dandonneau*, 1986, 1992], remotely sensed ocean color [*Dupouy-Douchement et al.*, 1993; *Halpern and Feldman*, 1994; *Leonard and McClain*, 1996], cruises [*Barber and Chavez*, 1983; *Murray et al.*, 1994; *Radenac and Rodier*, 1996; *Mackey et al.*, 1997], and moorings [*Foley et al.*, 1997]. *Barber and Chavez* [1983] showed the similar responses of sea surface temperature, nutrient, and production to the thermocline depth variations: nutrients and production decreased while SST rose when the thermocline sank. Low surface chlorophyll concentrations were also measured in the central and eastern Pacific during El Niño [*Dandonneau*, 1986, 1992]. During the U.S. Joint Global Ocean Flux Study (JGOFS) Equatorial Pacific Process Study (EqPac), chlorophyll and primary production were low in early 1992 when weak El Niño conditions prevailed [*Barber et al.*, 1996; *McCarthy et al.*, 1996]. In a recent study, *Friedrichs and Hofmann* [2001] show that the interannual variability of the thermocline depth was mainly responsible for the low production during these cruises, but that the low biomass level was rather the consequence of the lack of higher frequency processes such as tropical instability waves. In contrast with observations in the central and eastern Pacific, primary production in the western Pacific warm pool is higher during El Niño years [*Dandonneau*, 1986; *Radenac and Rodier*, 1996; *Leonard and McClain*, 1996; *Mackey et al.*, 1997].

During the 1997-1998 El Niño, a variety of newly acquired biological and physical data were available, broadening and deepening our insight of the basin-wide alteration of biogeochemistry during a strong ENSO event. *Chavez et al.* [1998] documented the perturbation of the phytoplankton biomass in the equatorial zone using physical and bio-optical sensors installed on a mooring at 0°, 155°W during the onset of the event. Recent studies [*Chavez et al.*, 1999; *Strutton and Chavez*, 2000] described the El Niño event and the subsequent recovery of the upwelling, and addressed the role of iron. *Murtugudde et al.* [1999] commented on the consequences of the event on biology using the Sea-viewing Wide Field-of-view Sensor (SeaWiFS) chlorophyll data and physical simulations. Observation-based studies are limited because of the scarcity of data (cruises, mooring) or because subsurface processes cannot be properly apprehended by synoptic sensors such as ocean color sensors. No mooring array, such as the TAO array [*Hayes et al.*, 1991; *McPhaden et al.*, 1998] that has been so helpful in monitoring and understanding the physical aspects of El Niño events, exists to study the chemical and biological disturbances. Modeling studies can complement in situ or remotely sensed studies to permit high spatial and temporal resolution.

Few modeling studies have addressed the coupling of physical dynamics and biology on the basin scale. Early studies using climatological forcing to force basin-wide physical-biological models aimed at characterizing the mean annual nitrate budget in the cold tongue of the Pacific Ocean [*Toggweiler and Carson*, 1995; *Chai et al.*, 1996]. Recently, a general circulation model forced with interannually varying winds drove a nitrate transport model [*Stoens et al.*, 1999] that was able to reproduce the main nitrate features observed during JGOFS cruises in 1994. Like in observations, the poor and low new production waters in the western Pacific are concomitant with the fresh warm pool waters. The same zonal advection processes that maintain and displace the salinity front explain the maintenance of this new production front and its huge ENSO-related zonal displacement during the 1992-1995 weak El Niño period [*Stoens*, 1998]. As the nitrate variability is much more controlled by the fast equatorial physical dynamics than by the slow-acting biological sink, only a 3-D approach can be used to understand variability in both regions. Yet, one shortcoming of the *Stoens et al.* [1999] study is the lack of strong interannual variability during the 1992-1995 time period.

In this paper, we use the same biogeochemical model as *Stoens et al.* [1999] along with satellite and in situ data to better understand how changes in nitrate and new production respond to the variability of physical processes during the exceptionally strong 1997-1998 El Niño and the subsequent La Niña. In particular, we examine the destruction of the equatorial east-west biogeochemical asymmetry in 1997 and its swift recovery in 1998. The data we use are presented in the next section, followed by the description of the ocean circulation and biological models in section 3. In section 4, observations and model outputs are used for a chronological description of the expansion and decline of El Niño

conditions in the equatorial Pacific during the 1997-1998 period. In section 5, we focus on the physical processes responsible for the evolution of nitrate and new production fields. Finally, concluding remarks are made in section 6.

2. Data

Numerous data are used in this study for forcing, description, and validation. Wind stresses are derived from the satellite-borne European Remote Sensing ERS-1 (January 1993 through May 1996) and ERS-2 (March 1996 through December 1998) scatterometers [*Bentamy et al.*, 1996]. Weekly wind stress global fields, originally on $1° \times 1°$ grid, are interpolated onto the model grid to force the ocean circulation model. The weekly *Reynolds and Smith* [1994] sea surface temperature (SST) is derived from both in situ and satellite data on a $1° \times 1°$ grid.

The climatological sea surface salinity (SSS) [*Delcroix*, 1998] is derived from bucket measurements on board merchant ships, from conductivity-temperature-depth (CTD) salinity, and from thermosalinograph measurements from merchant ships and from the TAO moorings during the1979-1992 years. It is on a 10° longitude by 2° latitude grid. The model SSS mean state and standard deviation computed over 1993-1998, which is the total period of the run, are validated against this climatology.

Delcroix et al. [1998] described SSS along the Fiji-Japan route. This shipping route crosses the equator between 170°E and 175°E. Monthly averaged in situ SSS between 0.5°S and 0.5°N and between170°E and 175°E are compared to the corresponding modeled SSS in order to examine the accuracy of the modeled zonal displacement of the fresh pool. Gaps in the observed SSS are filled using a Laplacian interpolation.

The TOPEX/Poseidon sea level anomaly data are 10-day fields built onto a $1° \times 1°$ grid [*Tapley et al.*, 1994]. Interannual anomalies are computed relative to the 1993-1996 seasonal cycle following *Boulanger and Menkes* [1999].

Temperature and zonal currents from the equatorial TAO moorings [*Hayes et al.*, 1991; *McPhaden et al.*, 1998] provide information about the oceanic vertical structures. Currents derived from mechanical current meters and from acoustic Doppler current profilers are merged. Data gaps are filled according to *McCarty and McPhaden* [1993]. For the validation of the model, 5-day averages are calculated from the daily TAO data. At each TAO mooring position, mean and standard deviation of observed and modeled values are computed when measurements are available.

Ocean color data are instrumental in monitoring the temporal evolution of surface structures. Polarization and Directionality of the Earth Reflectances (POLDER) [*Deschamps et al.*, 1994] and Ocean Color and Temperature Scanner (OCTS) sensors were launched in August 1996 aboard the ADEOS satellite. Data acquisition unfortunately stopped on June 30th, 1997, due to a satellite failure. The following ocean color mission, SeaWiFS, provided data starting in late September 1997. No ocean color data were available during the summer of 1997. To obtain the best possible monitoring of the biological activity in the equatorial Pacific, we used POLDER data during the onset of the 1997-1998 El Niño and SeaWiFS data during the peak and the decline of the event. We preferred POLDER to OCTS because the latter was forced to tilt on each orbit to avoid Sun glint. This tilt generated a "blind zone" which coincided with the equator in March and April. In this study we use weekly SeaWiFS and 10-day POLDER composites of the chlorophyll concentration on a $^1/_3° \times ^1/_3°$ grid. The last POLDER ocean color reprocessing is done using the SeaWiFS OC2 bio-optical algorithm to estimate chlorophyll concentration from marine reflectances. This OC2 algorithm [*O'Reilly et al.*, 1998] is based on the ratio of the diffuse marine reflectances at 490 and 565 nm. We believe that the use of a single bio-optical algorithm ensures a better continuity between the two data sets.

To validate the modeled surface nitrate, both climatological and cruise data are used. Climatological nitrate concentrations are produced on a $1° \times 1°$ grid as the result of an objective analysis of data collected between 1900 and 1992 [*Conkright et al.*, 1994]. The historical data set of surface nitrate measurements compiled by *Chavez et al.* [1996b] spans the equatorial Pacific east of the date line essentially during the 1980s. It is completed by additional nitrate measurements collected in the western Pacific and during the 1990s. Sources for the additional data include World Ocean Circulation Experiment (WOCE) cruises (along 179°E in August 1993, along 110°W in April 1994, and along 170°W in February-March 1996), JGOFS-France cruises (along 165°E and the equator in September-October 1994, along 150°W in November 1994 [*Dandonneau*, 1999], and along 180° in November 1996), and the Institut de Recherche pour le Développement (IRD) / US-JGOFS joint cruise along the equator in April-May 1996 [*Le Borgne et al.*, 1999]. During the 1980s and 1990s, cruises were completed in the western Pacific by the Commonwealth Scientific and Industrial Research Organisation (CSIRO) [*Mackey et al.*, 1997], and by IRD along 165°E [*Radenac and Rodier*, 1996]. A long-term mean surface modeled nitrate concentration and its standard deviation have been computed over 1993-1998. They are compared to the climatology and cruise data at specific locations, essentially when repeated cruises have been undertaken.

3. The Coupled Ocean Circulation-New Production Model

The model used is very similar to that of *Stoens et al.* [1999]. It differs by the time period it encompasses, the heat and freshwater fluxes used to force the physical model, and the coarser horizontal grid resolution.

3.1. Ocean Circulation Model

The ocean circulation model used in this study has already been described by *Vialard et al.* [2001]. This general circulation model (GCM) covers the tropical Pacific between 120°E and 75°W, and between 30°N and 30°S. The zonal resolution is 1°, and the meridional resolution varies from 0.5° between 5°N and 5°S to 2° at the northern and southern boundaries. The vertical resolution is 10 m over the first 150 m. A vertical mixing scheme based on a prognostic turbulent kinetic energy equation [*Blanke and Delecluse*, 1993] is applied.

Wind stresses derived from ERS-1 and ERS-2 scatterometers [*Grima et al.*, 1999] are used. Heat and freshwater fluxes are based on a seasonal cycle constructed from the 1979-1993 average of European Centre for Medium-Range Weather Forecasts (ECMWF) reanalysis [*Gibson et al.*, 1997]. A -40 W m^{-2} K^{-1} relaxation toward the *Reynolds*

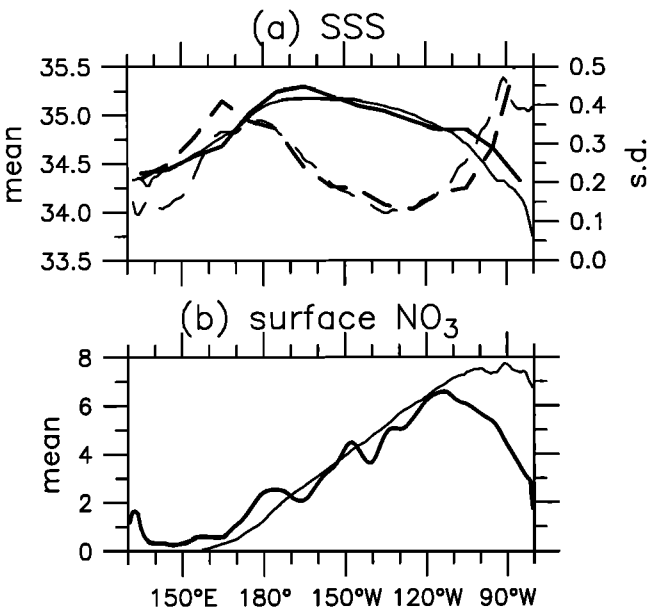

Figure 1. Data for the equatorial band (1°S-1°N): (a) Mean and standard deviation of sea surface salinity (SSS) in practical salinity unit (psu). The thick solid line is the climatological SSS during 1972-1992 [*Delcroix*, 1998], and the thin solid line is the modeled SSS averaged over 1993-1998. The thick dashed line is the standard deviation of the monthly climatological SSS, and the thin dashed line is the standard deviation of the modeled SSS. (b) Surface nitrate (μM). The thick line is the climatological nitrate [*Conkright et al.*, 1994], and the thin line is the modeled nitrate concentration averaged over 1993-1998.

and Smith [1994] SST is included in the surface flux formulation. No relaxation toward observed SSS is applied. Instead, a freshwater flux correction constrains the model to *Levitus* [1982] climatology. This flux correction term is derived as by J. Vialard et al. (A modeling study of salinity variability and its effects in the tropical Pacific ocean during the 1993-1999 period, submitted to *Journal of Geophysical Research*, 2001, hereinafter cited as J. Vialard et al., submitted manuscript, 2001). It is spatially variable but constant in time and is of the order of the uncertainty on the surface fluxes. This version of the model successfully reproduced the main features of the tropical Pacific mean state and variability over 1993-1998 [*Vialard et al.*, 2001], making it suitable to force the nitrate model described in the next section.

3.2. Nitrate Model

Here, we briefly describe the biological model, which is detailed by *Stoens et al.* [1999]. The form of the tracer advection-diffusion equation is

$$\partial_t \mathrm{NO3} = -u\partial_x \mathrm{NO3} - v\partial_y \mathrm{NO3} - w\partial_z \mathrm{NO3} + D_h \Delta_h(\mathrm{NO3}) + \partial_z(K_z \partial_z \mathrm{NO3}) + \mathrm{S}.$$

The left-hand term represents the total nitrate tendency. The first three terms on the right-hand side are the zonal, meridional, and vertical advection, respectively. The fourth and fifth terms are the horizontal diffusion (parameterized by the horizontal Laplacian operator Δ_h), and the vertical diffusion. All the physical variables such as the zonal velocity (u), the meridional velocity (v), the vertical velocity (w), and the vertical diffusion coefficient (K_z) are 5-day outputs of the ocean circulation model. The horizontal eddy coefficient D_h is the same as the one used in the physical model [*Vialard et al.*, 2001]. The biological model consists of a simple nitrate sink, S, calculated in the euphotic layer. The nitrate uptake is biomass dependent and has the following form:

$$S = -V_{\max} \frac{\mathrm{NO3}}{\mathrm{NO3} + K_{\mathrm{NO3}}} \frac{\mathrm{PUR}}{\mathrm{PUR} + K_E} [\mathrm{Chl}].$$

The photosynthetic usable radiation (PUR) is deduced from the shortwave downward radiation as explained by *Stoens et al.* [1999]. The value of the half saturation constant for PUR, K_E, is 70×10^6 mol photon m^{-2} s^{-1}, as chosen by *Stoens et al.* [1999]. $V_{\max}$ (3 μmol NO_3 mg Chl^{-1} s^{-1}) and K_{NO3} (0.01 μM) are the maximum nitrate assimilation rate and the half-saturation concentration. They are adjusted to retrieve modeled vertical nitrate sections that agree the best with concurrent observed nitrate vertical sections. The chlorophyll concentration (Chl) calculation is described by *Stoens et al.* [1999]. First, the surface chlorophyll is derived from a statistical relationship between the surface nitrate and chlorophyll. Then, the vertical profile of chlorophyll is calculated following a method proposed and validated by *Morel and Berthon* [1989]. The surface relationship, based on nitrate-chlorophyll statistics specific to the tropical Pacific region, is loose [*Stoens*, 1998]. Nevertheless, chlorophyll and nitrate concentrations are always positively correlated in the equatorial Pacific, as confirmed by recent surface measurements collected between Panama and Tahiti on board merchant ships (Y. Dandonneau, personal communication, 2001]. This relationship, which is not tight at mesoscale or smaller scale, is valid at large scale and can be used in such a study. Below the euphotic layer (90 m), the new production is exported following the vertical profile of *Honjo* [1978], and is locally and instantaneously remineralized into nitrate.

The model is initialized with the Levitus climatological nitrate field. The spin-up of the model is reached by repeating the first year of simulation (1993). In the equatorial (2°S-2°N) region, the equilibrium of the nitrate annual cycle in the euphotic layer is achieved after eight years of simulation. At that time, the nitrate change per year is less than 2% in the euphotic layer of the equatorial region. Then, the nitrate model is forced with outputs of the physical model during the following years.

3.3. Validation of Mean Large-Scale Structures

Because there is a heat flux correction term, a detailed validation against the Reynolds SST data is pointless. Nevertheless, even with this correction term, the mean modeled SST in the eastern basin may be more than 1°C warmer than the observed SST, in particular during the peak period of the event (not shown). Validation against SSS observations is only pertinent in terms of modeled variability as the water fluxes have been corrected with a constant term.

In the equatorial band, the western and eastern Pacific are occupied by low-salinity waters with SSS increasing in the center of the basin (Figure 1a). The mean salinity front at the eastern edge of the warm pool appears with a sharper zonal gradient than the transition between low-salinity waters of the Central America coasts and the saltier waters of the cold tongue. This average SSS distribution is the result of the mean evaporation/precipitation pattern [*Delcroix et al.*, 1996], but

Table 1. Comparison of the Observed Mean Values of Surface Nitrate with the 1993-1998 Mean Modeled Nitrate Concentrations at the Equator[a]

Longitude	Average, μM		Standard Deviation, μM		Number of Observations
	Cruises	Model	Cruises	Model	
95°W	6.51	6.83	3.01	2.93	75
110°W	6.77	6.63	3.08	2.69	143
120°W	5.93	5.90	2.69	2.47	18
140°W	4.67	4.39	2.10	1.92	88
150°W	3.89	3.64	1.41	1.73	138
170°W	2.22	2.03	1.55	1.25	34
165°E	0.34	0.25	0.77	0.54	206
155°E	0.03	0.03	0.07	0.11	191
137°E	0.08	0.00	0.11	0.00	47

[a]The origin of cruises is detailed in the text. Nitrate is extracted in 4° longitude × 4° latitude boxes centered at the given longitude and at the equator.

also of the surface current. Actually, the zonal convergence of the salty water of the cold tongue driven westward by the South Equatorial Current (SEC), with the fresher, eastward flowing warm pool water is a main contributor to the maintenance of the salinity front at the eastern edge of the warm pool. The SSS variability is well reproduced (Figure 1a). The region of zonal migration of the eastern edge of the warm pool is evidenced by a peak of variability between the date line and 160°E both in the model and in the observations. Further east, the variability decreases between 160°W and 110°W, probably because the effects of the horizontal salt advection counteract the effects of the vertical salt advection on a seasonal timescale [*Delcroix and Picaut*, 1998]. Then, the variability increases eastward.

West of 110°W, the mean zonal distribution of the modeled surface nitrate is consistent with the climatology (Figure 1b) and cruises (Table 1). West of 165°E, both the model and observations show the nitrate-depleted surface layer characteristic of the oligotrophic warm pool. The increase of the mean nitrate concentration modeled east of 165°E is close to the measured one. Yet, east of the Galapagos Islands, both the climatology and cruises show a decrease of the nitrate concentration that is not reproduced by the model. The modeled nitrate variability is very weak in the warm pool region in the model and observations and rises east of 165°E (Table 1).

Zonal current is the key factor in maintaining the front at the eastern edge of the warm pool [*Picaut et al.*, 1996; *Vialard and Delecluse*, 1998]. Thus a validation of the modeled zonal current at TAO moorings over the 1993-1998 period is shown in Table 2. The modeled mean surface zonal velocity is in good agreement with the TAO data. The westward flowing SEC spans the central and eastern basins. The surface current reverses or approaches zero west of 165°E. This is the convergence region described by *Picaut et al.* [1996] and *Vialard and Delecluse* [1998]. At that location, the mean modeled zonal current is particularly accurate compared with observations. In the eastern Pacific, the modeled SEC diverges from observations and is too strong. This is confirmed by the comparison of the modeled surface currents to the 1987-1992 surface current observations of *Reverdin et al.* [1994]. Modeled and observed (TAO) variability compare well except at the easternmost mooring location.

Vialard et al. [2001] found a too diffuse thermocline in a model experiment very close to this one. Similarly, we find that the modeled nitracline is more diffuse than in cruise data. Modeled nitrate values are consistent with observations in the surface layer, but the modeled concentrations are too low in the bottom part of the thermocline. Similar features are illustrated by *Stoens et al.* [1999] in the equatorial section (see their Figures 5d and 5i). Comparing the modeled nitrate meridional sections with cruises at 155°W in November 1997 and June 1998 [*Strutton and Chavez*, 2000] leads to the same conclusions (not shown). This discrepancy might be linked to the imperfect mixing scheme that causes the thermocline to be

Table 2. Statistics of Concurrent Modeled and Observed Surface Zonal Currents at the Equatorial Tropical Atmosphere-Ocean (TAO) Moorings Location During the 1993-1998 Period

Longitude	Average, m s^{-1}		Standard Deviation, m s^{-1}		Correlation Coefficient
	TAO	Model	TAO	Model	
110°W	-0.03	-0.11	0.39	0.25	0.65
140°W	-0.12	-0.10	0.36	0.30	0.74
170°W	-0.15	-0.16	0.29	0.30	0.81
165°E	0.00	0.00	0.37	0.37	0.86
156°E	0.08	0.02	0.26	0.28	0.77
147°E	-0.04	-0.07	0.30	0.29	0.77

Table 3. Some Literature Values of the Nitrate Uptake in Oligotrophic and Mesotrophic Regimes of the Tropical Pacific

Region	Reference	Nitrate Uptake, mmol NO_3 m^{-2} d^{-1}
	Oligotrophic Regime	
warm pool (model)	*Peña et al.* [1994]	0.52
140°W, 5°S-12°S	*McCarthy et al.* [1996]	0.2-1
140°W, 3°N-12°N	*McCarthy et al.* [1996]	0.2-1
167°E, 0°	*Navarette* [1998]	1.2
150°W, 11.5°S-16°S	*Raimbault et al.* [1999]	0.47-1.58
	Mesotrophic Regime	
150°W, 0°	*Dugdale et al.* [1992]	1.43
133°W, 2°N-2°S	*Peña et al.* [1992]	2.85
150°W, 1°N-1°S (2-D model)	*Carr et al.* [1995]	4.3
90°W-180°, 5°S-5°N	*Chavez et al.* [1996a]	2.0-3.0
140°W, 2°N-2°S	*McCarthy et al.* [1996]	2.8
150°W, 0°	*Navarette* [1998]	3.0
150°W, 5°S-1°N	*Raimbault et al.* [1999]	1.65-2.68
90°W-180°, 5°S-5°N (model)	*Toggweiler and Carson* [1995]	3.3
90°W-180°, 5°S-5°N (model)	*Chai et al.* [1996]	2.3

too diffuse in the physical model and the nitracline to be too diffuse here. Most probably, this leads to the underestimation of the nitrate variability at depth, because the amplitude of the local changes caused by vertical movements of the nitrate maximum will be reduced. In the very east of the equatorial Pacific, the subsurface increase of the nitrate concentration reported in climatology [*Conkright et al.*, 1994] or in cruise data [*Reverdin et al.*, 1991] is overestimated in the model.

Despite some caveats, the model achieves a fairly realistic representation of the oceanic variability and of nitrate conditions in the warm pool and in the cold tongue. While agreement of modeled and observed new production values are expected, new production measurements are scarce, with only a few cited values available (Table 3). In the oligotrophic region, the modeled new production is always lower than 1 mmol NO_3 m^{-2} d^{-1}, which is consistent with the literature values. The weak maximum observed near the nitracline [*Navarette*, 1998] is reproduced in modeled new production profiles (not shown). Above this maximum, methodological problems related to the low nitrate concentration may explain why the model new production is lower than the measured nitrate uptake. For the mesotrophic regime, the modeled new production ranges between 1.7 and 2.6 mmol NO_3 m^{-2} d^{-1} during 1993-1996 in the 130°W-150°W region, and the 1993-1996 average in the *Wyrtki* [1981] box (5°S-5°N; 90°W-180°) is 1.9 mmol NO_3 m^{-2} d^{-1}. These estimates of the new production are slightly lower than those inferred from measurements or from other ecosystem models (Table 3), and modeled new production profiles are generally weaker than the measured profile of nitrate uptake at 150°W [*Navarette*, 1998].

Measurements in the tropical Pacific yield a relationship between new production and the nitrate concentration integrated over the euphotic layer (Figure 2) [*Raimbault et al.*, 1999]. In the model, such a dependence (Figure 2) is expected, as nitrate is the only nutrient considered. In agreement with observations, the slope of the relationship is weak for nitrate concentrations characteristic of the cold tongue. For a fivefold increase of nitrate, the new production increases only by about 50%. The agreement of the modeled relationship with the one deduced from observations gives confidence in the model.

4. Equatorial 1997-1998 El Niño: Data and Model

The 1997-1998 El Niño was described as the major El Niño of the twentieth century [*McPhaden*, 1999]. It was the best observed warm event owing to in situ and satellite measurements. The model is used here to complement sparse

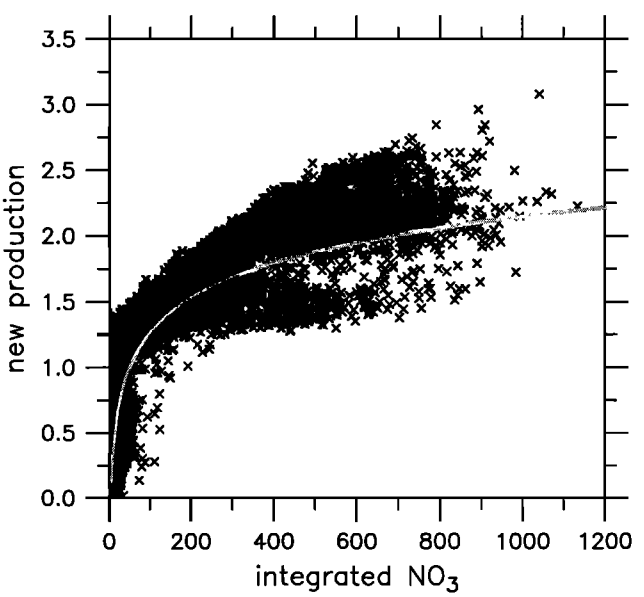

Figure 2. Relationship between the new production (mmol N m^{-2} d^{-1}) and the nitrate content integrated over the euphotic layer (μM). Crosses are the modeled values at the equator. The shaded line is the relationship found by *Raimbault et al.* [1999] in the equatorial Pacific.

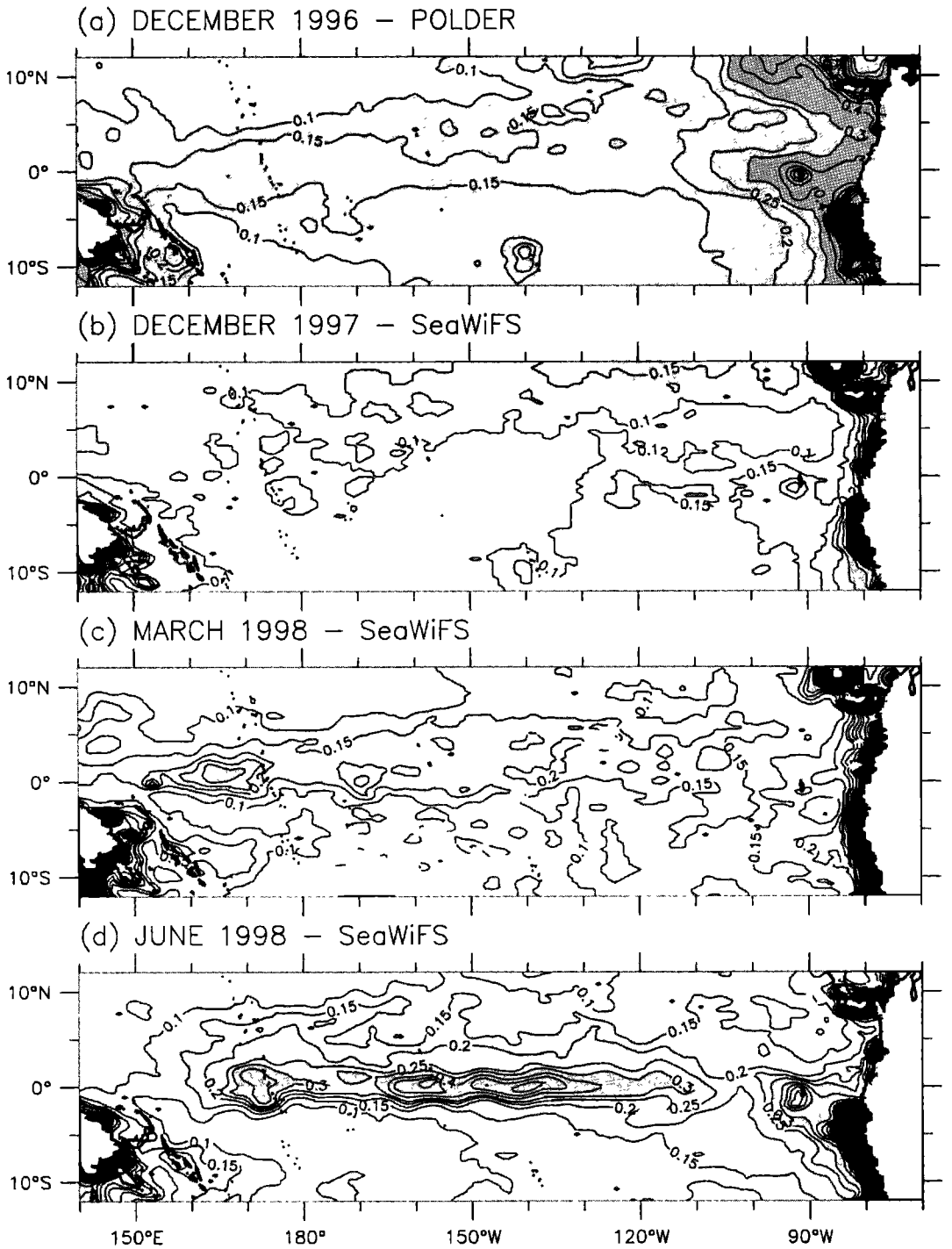

Figure 3. Maps of monthly mean chlorophyll concentrations (mg m^{-3}) derived from (a) POLDER and (b-d) SeaWiFS. Regions with chlorophyll between 0.1 and 0.3 mg m^{-3} are lightly shaded, and contours are every 0.05 mg m^{-3}. Regions with chlorophyll higher than 0.3 mg m^{-3} are darkly shaded, and contours are every 0.1 mg m^{-3}.

observations and allows us to analyze the links between the evolution of the biological and physical parameters.

4.1. November 1996 Through June 1997: The Growth of the El Niño Event

At the end of 1996, the equatorial enriched region extended far into the west, as seen in the POLDER data of December 1996 (Figure 3a) and reproduced in the model (Figure 4a). The measured concentration of surface nitrate was representative of cold conditions in the central Pacific (170°W or 155°W), and the modeled nitrate appears to be underestimated by more than 1 μM (Table 4). While the ocean was in this weak La Niña state, a series of westerly wind events occurred in the western Pacific (Figure 5a). In this region, the surface chlorophyll increased (Figure 5d) when the wind bursts blew (December 1996, March 1997, and April 1997). The response of the ocean to the first wind burst in December 1996 was a downwelling Kelvin wave (dashed

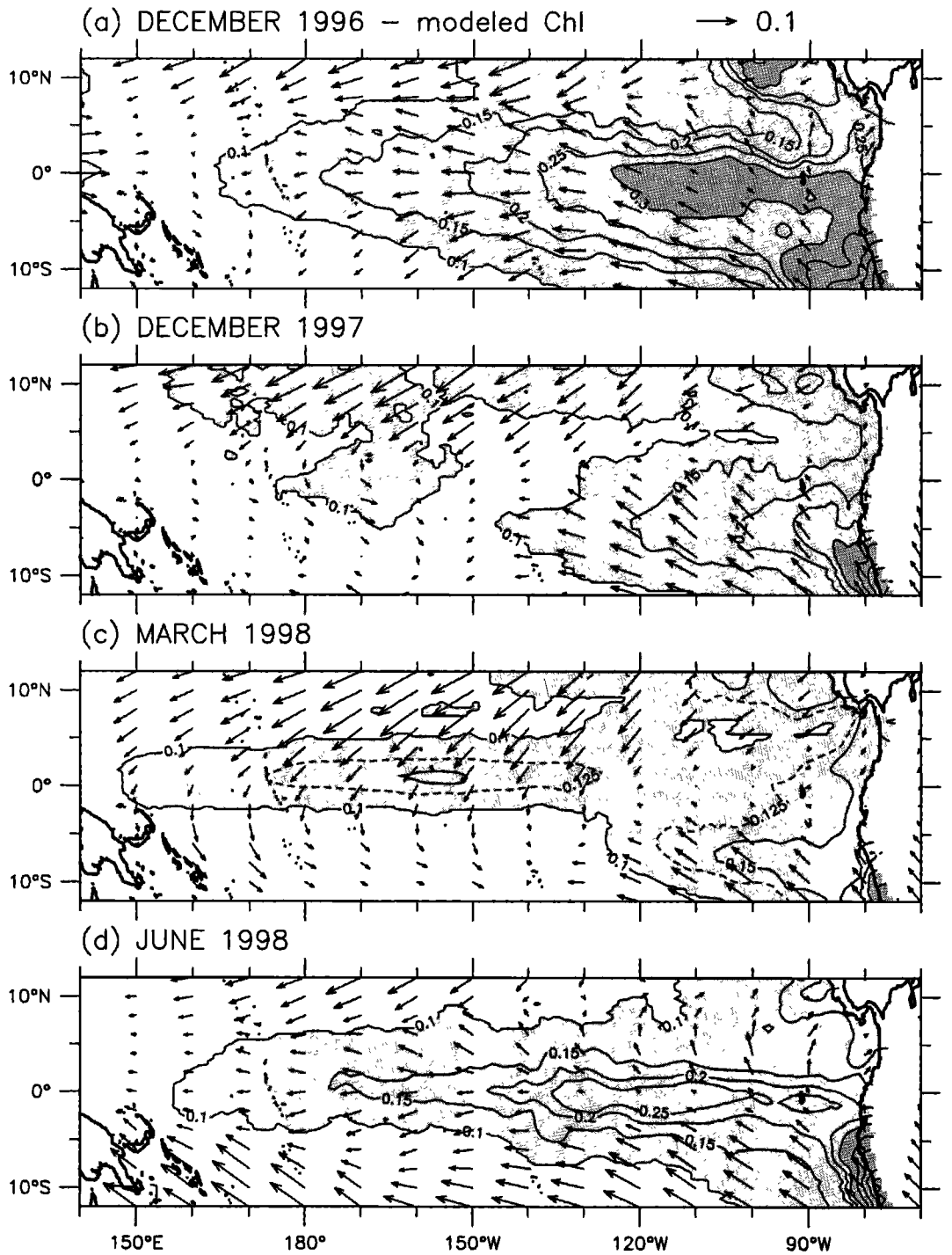

Figure 4. Maps of monthly mean modeled surface chlorophyll concentrations (mg m^{-3}) and ERS wind stress (N m^{-2}). Shading and contours as in Figure3. In March 1998, the 0.125 mg m^{-3} isoline (dashed) has been added to emphasize the dawning upwelling.

line in Figure 5). Eastward surface currents were generated along its track in the observations and in the model (Figure 6). In January 1997, this Kelvin wave reached 155°W, where the deepening of the thermocline and a slight decrease of the chlorophyll concentration in the upper 20 m were recorded at the mooring deployed at that location [*Chavez et al.*, 1998]. Then, both the thermocline depth and the chlorophyll recovered. The strong westerly wind burst of March 1997 in the western Pacific (Figure 5a) triggered a second Kelvin wave (Figure 5). The associated eastward surface current that reached 110°W in April 1997 is well reproduced (Figure 6). This Kelvin wave initiated a rapid eastward displacement of the eastern edge of the warm pool. The 29°C surface isotherm that marks the eastern edge of the warm pool was at 170°W in March and reached 140°W in June (Figure 5c). During this period, observations and model values along the Fiji-Japan shipping route (Figure 7) show a SSS decrease that was a consequence of the eastward extension of the fresh warm

Table 4. Observed and Modeled Surface Nitrate at the Equator in 1996-1998[a]

	Cruises at 155°W	Model at 155°W	Cruises at 170°W	Model at 170°W
Nov. 1996			4.3[b]	2.8-2.1
Dec. 1996	5.1[b]	3.4-3.9		
Jan. 1997	5[c]	3.9-3.7		
May 1997	3[b,c]	2.1-2.0	0[b]	0
Nov. 1997	< 0.05[c]	0		
June 1998	4[b]	2.4-3.3		

[a] Units are micromolars.
[b] Observed concentrations are derived from *Strutton and Chavez* [2000].
[c] Observed concentrations are derived from *Chavez et al.* [1999].

pool. At the 155°W mooring, the chlorophyll concentration decreased in March-April. The surface nitrate concentration was estimated to fall from about 5 μM (4 μM in the model, Figure 8b) in early March to 3 μM (2 μM in the model) 2 months later [*Chavez et al.*, 1998]. In May 1997, the nitrate depletion in the surface layer at 170°W is well simulated (Table 4). In the model, low new production waters progress toward the eastern equatorial Pacific, and the biological front follows the SSS front indicated by the 35.8 practical salinity unit (psu) isoline in Figure 8a. In the POLDER time series, the eastern edge of a zone of low chlorophyll content (lower than 0.15 mg m^{-3}) in the western Pacific shifted eastward from about 170°E in March-April 1997 and reached 155°W in June (Figure 5d). This migration was reminiscent of the eastward displacement of the front in late 1994 described by *Eldin et al.* [1997] and modeled by *Stoens et al.* [1999]. However, this front migration was much faster and broader than in 1994 (the displacement of the 28°C surface isotherm of the *Reynolds and Smith* [1994] analysis was 60° longitude in 105 days in 1997 versus 20° in 120 days in 1994).

4.2. July-October 1997: A Short Pause

This progression paused at the end of summer (Figure 5c). According to *Boulanger and Menkes* [1999], westward surface current associated with a first-mode downwelling Rossby wave, resulting from local wind forcing and eastern boundary reflection of downwelling Kelvin waves, overcame the eastward surface current associated with the downwelling Kelvin wave. It finally resulted in a westward displacement of the warm pool edge. The brief cessation of the strong anomalous eastward flow in the central Pacific in July-August 1997 is correctly simulated (Figure 6d).

In autumn 1997, the downwelling Kelvin wave signal dominated again in response to strong westerly wind anomalies that had developed in the central Pacific (Figure 5a). As a consequence, the surface current remained eastward over most of the equatorial basin (Figure 8d), and the eastward expansion of the biologically poor warm pool resumed. In September 1997, the SeaWiFS images show that the low-chlorophyll waters (<0.1 mg m^{-3}) have indeed moved eastward (Figure 5d) together with the warm pool region (Figure 5c).

4.3. November 1997 Through January 1998: The Mature Phase

At the end of the year, surface waters warmer than 28°C (Figure 5c) spanned the entire equatorial Pacific basin and the Equatorial Undercurrent (EUC) has almost totally disappeared. In November 1997 at 155°W, the surface layer was nitrate depleted (Table 4), and the nitracline was around 100 m depth both in situ [*Strutton and Chavez*, 2000] and in the model (Figure 9b). The euphotic layer in the central Pacific was entirely nitrate depleted (Figure 8c). December 1997 was the period when the equatorial region was the less biologically active as seen by the SeaWiFS data (Figures 5d and 3b) or the model (Figure 4b). The observed and modeled nitrate-poor equatorial waters were at their maximum eastward expansion. During the 1997 peak period, oligotrophic conditions stretched from the western basin to 130°W, with satellite and modeled chlorophyll lower than 0.1 mg m^{-3} (Figures 3b, 4b, and 5d) and surface waters warmer than 29°C (Figure 5c). The surface enriched region, confined to the east of 130°W, had low chlorophyll content (about 0.15 mg m^{-3}) and modeled new production (about 1.5 mmol NO_3 m^{-2} d^{-1}) (Figure 8a). Such a general decrease has already been documented during the strong 1982-1983 El Niño and, to a lesser extent, during the moderate 1986-1987 event [*Dandonneau*, 1992]. Chlorophyll and nitrate profiles sampled along 155°W in November 1997 [*Strutton and Chavez*, 2000] were representative of the warm pool conditions described by *Navarette* [1998]. Indeed, during the peak of the event, conditions in the central Pacific were oligotrophic, and the region was nitrate limited.

Nevertheless, at the end of this period, signs of the weakening of the event started to appear. Easterly winds resumed in December 1997 (Figure 5a). The very abrupt surface current reversal almost everywhere in the equatorial basin is well reproduced (Figures 6 and 8d). At that time, the sea level anomaly diminished (Figure 5b) and the SSS began to increase close to 170°E (Figure 7), sign of a westward retreat of the fresh pool. The chlorophyll concentration (Figure 5d) began to increase slowly, and new production (Figure 8a) started to increase after January 1998 in the western and central Pacific. The subsurface nitrate concentrations increase (Figure 8c) that started in December-January will condition the termination of El Niño.

4.4. February-May 1998: The Decay of the El Niño Event

In early 1998, both the thermocline and nitracline were flat and shallow along the equator (Figure 9c). Easterly winds that strengthened between 140°W and 170°E (Figure 5a), presented a strong northerly component (Figure 4c). The consequence of such a horizontal wind stress distribution was a northward displacement of the upwelling [*Cromwell*, 1953; *Charney and Spiegel*, 1971]. This enrichment was apparent in the surface chlorophyll field of both the model (Figure 4c) and SeaWiFS observations (Figure 3c) [*Murtugudde et al.*, 1999] as a chlorophyll-rich band centered north of the equator

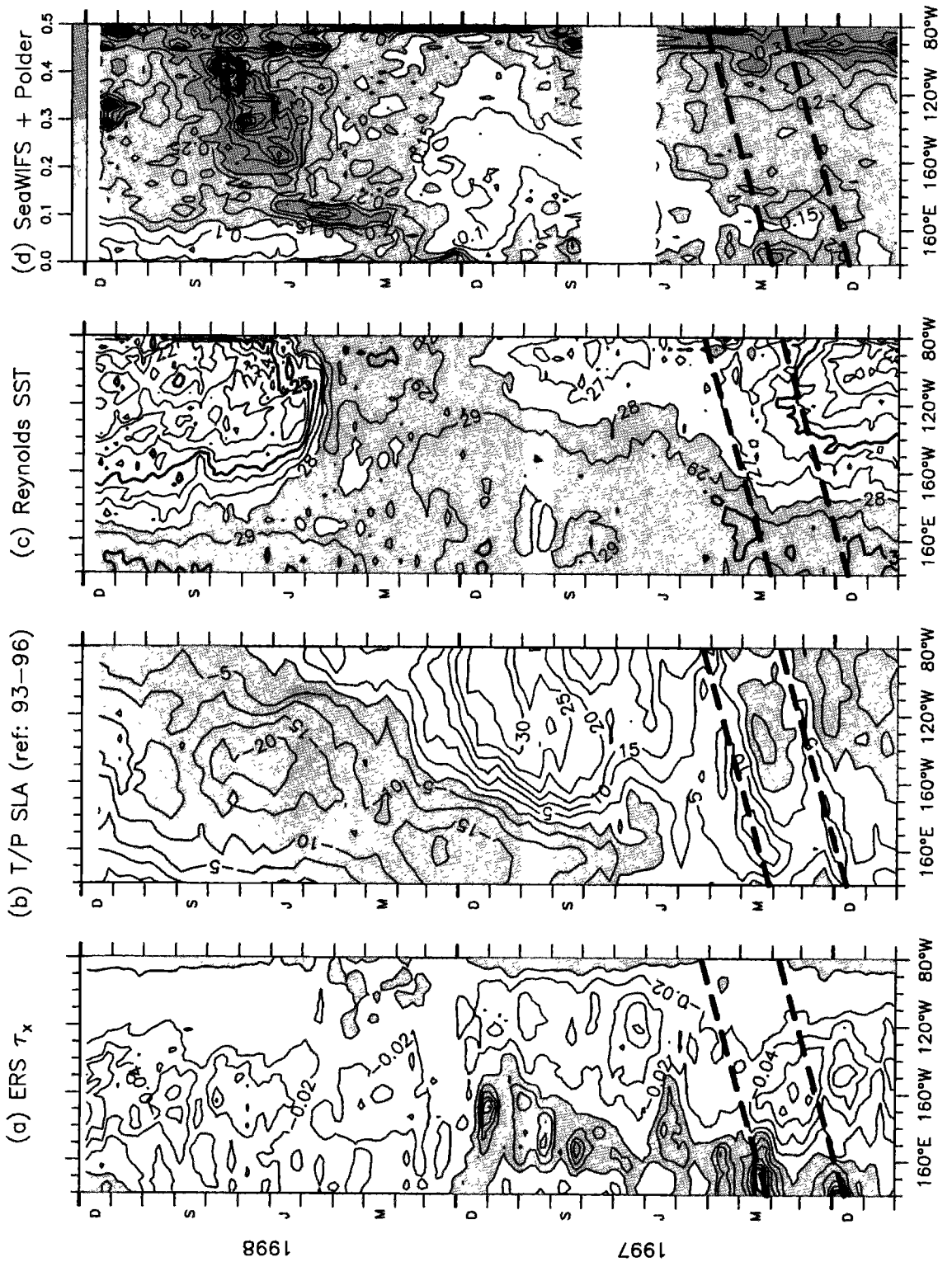

Figure 5. Time-longitude diagrams in the 2°S-2°N band. (a) ERS zonal wind stress (N m^{-2}). Eastward winds are shaded; contours are every 0.02 N m^{-2}. (b) TOPEX/Poseidon sea level anomaly (centimeters). Negative anomaly is shaded; contour interval is 5 cm. (c) *Reynolds and Smith* [1994] sea surface temperature (SST). SST greater than 28°C is shaded; contour interval is 1°C. (d) chlorophyll concentration derived from POLDER and SeaWiFS (mg m^{-3}). Contour interval is 0.05 mg m^{-3}. The dashed lines represent the downwelling Kelvin waves generated in December 1996 and in March 1997.

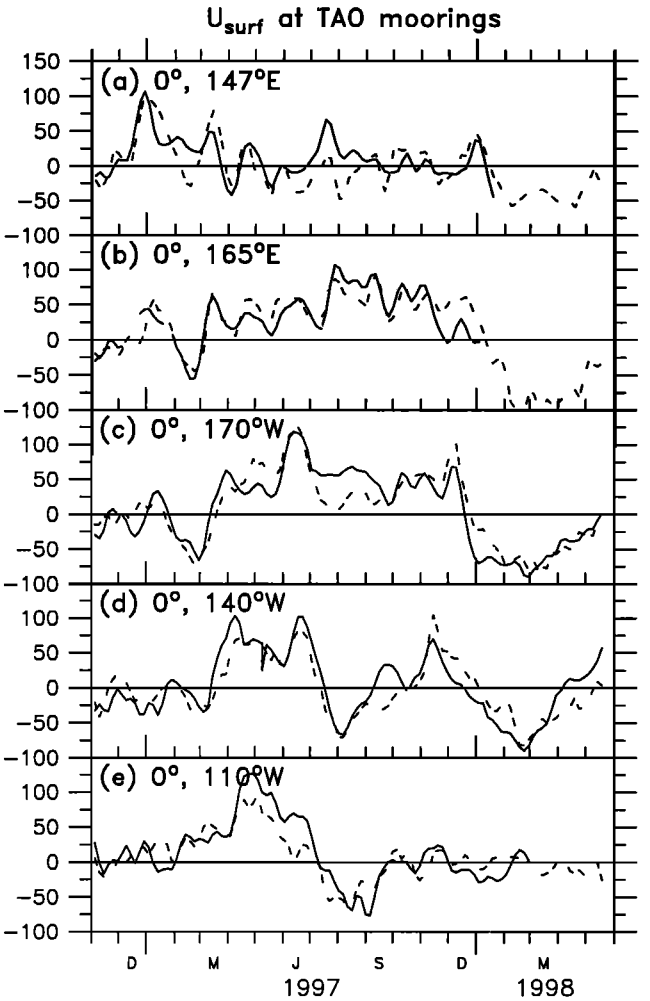

Figure 6. Comparison between the zonal current (cm s^{-1}) measured at TAO moorings (solid line) in the surface layer and the corresponding modeled value (dashed line) for (a) 147°E at 30 m, (b) 165°E at 15 m, (c) 170°W at 35 m, (d) 140°W at 25 m, and (e) 110°W at 25 m.

from the western boundary to 110°W. In the model, nitrate bursts reached the surface at the equator in March-April 1998 (Figures 8b and 9d), and the surface nitrate and new production increased west of 120°W. Further east, weak westerlies were still blowing (Figure 5a), and surface nitrate and new production remained low (Figures 8a and 8b).

A chlorophyll bloom was confined around 165°E between February and June 1998 in the SeaWiFS data (Figures 3d and 5d) [*Murtugudde et al.*, 1999]. This small-scale bloom that seemed to be distinct from the equatorial enrichment does not appear in the model surface outputs (Figure 4d).

4.5. June-December 1998: La Niña Conditions

In May-June 1998, trade winds have recovered over the entire equatorial Pacific (Figure 5a), and the northerly component has vanished (Figure 4d). The sea level anomaly was strongly negative in the central Pacific (Figure 5b) and the vertical distribution of nitrate was recovering along the equator (Figure 9e). As the equatorial upwelling strengthened, the SST decreased rapidly (Figure 5c), and an about 4-month chlorophyll bloom with concentrations as high as 0.4 mg m^{-3} showed up in SeaWiFS data in the central and eastern Pacific (Figures 5d and 3d) [*Murtugudde et al.*, 1999]. Data from cruises showed upwelling-type profiles at 155°W in June 1998 [*Strutton and Chavez*, 2000] with surface nitrate concentration over 4 μM (about 0.6 μM more than the climatology [*Conkright et al.*, 1994]), and chlorophyll concentration greater than 0.3 mg m^{-3} in the euphotic layer. The 1997-1998 El Niño turned into a strong La Niña event. Yet, in the simulation, the return of the biological activity has considerably less amplitude (Figure 4d), and the modeled new production only returns toward seasonal values in the central and eastern Pacific (Figure 8a). As La Niña conditions settled, the modeled enriched cold tongue extended to the western Pacific (Figure 8). Such a situation has already been reported at 165°E in April 1988, at the beginning of the strong 1988 La Niña event [*Radenac and Rodier*, 1996]. Surface nitrate concentrations were over 3 μM, and the surface chlorophyll was about 0.3 mg m^{-3} while the local wind was easterly. In terms of new production, the 1998 La Niña conditions build up as soon as January in the western Pacific, and the development was fully grown in June.

In section 3, we showed that the physical dynamics, nitrate mean states, and their variability defined from climatology or cruises are correctly simulated in the model. In this section, it has been shown that the physical and biogeochemical models qualitatively reproduce the observed departure from the mean state during the intense 1997-1998 event. In particular, the impact of the Kelvin waves on the modeled surface current is remarkably accurate. So, despite the shortcomings we mentioned, the model is capable of representing the variability of physical parameters and nitrate or new production large-scale features. Nevertheless, the simulated variability lacks amplitude, and bloom conditions are not fully reproduced. Keeping in mind the flaws and capabilities of the model, we can now turn to the 1997-1998 El Niño to analyze the processes responsible for biogeochemical variability.

5. Vertical Processes Versus Horizontal Processes in the Euphotic Layer

Navarette [1998] carefully described the warm pool and the upwelling regimes. For both regimes, light and nutrients are essential to new production. Whether the limitation of phytoplankton growth comes from light or from nutrients will define the regimes. In Figure 10, we show the evolution of the modeled new production in two layers during 1997-1998.

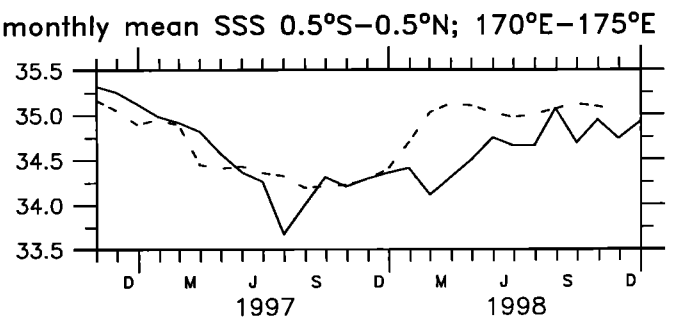

Figure 7. Comparison between the SSS (psu) derived from the Fiji-Japan shipping line (solid line) and the model (dashed line) averaged in the 0.5°S-0.5°N, 170°E-175°E region.

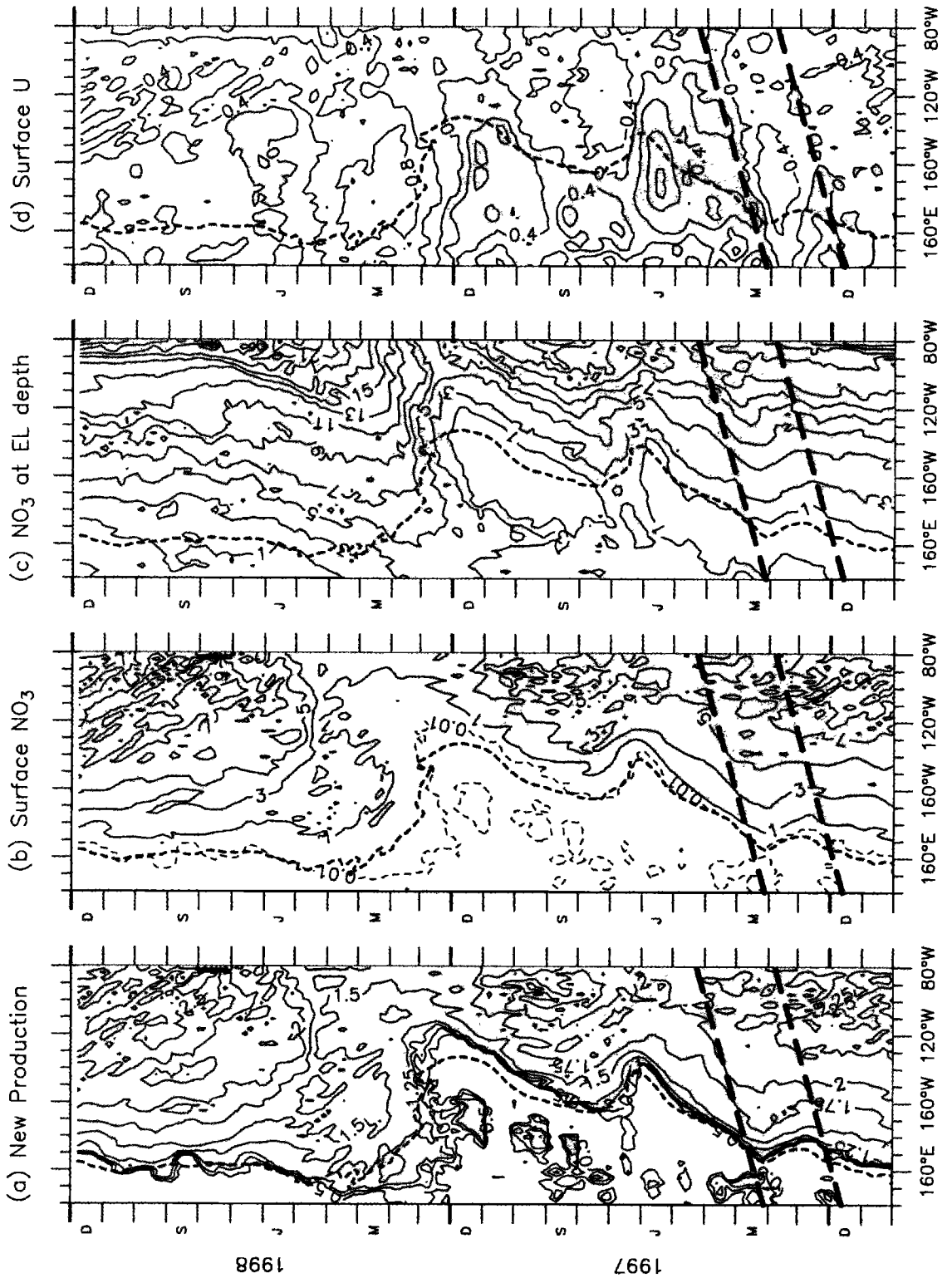

Figure 8. Time-longitude diagram of the model outputs along the equator. (a) New production (mmol N m^{-2} d^{-1}). Contour interval is 0.25 mmol N m^{-2} d^{-1}. (b) Surface nitrate (μM). Nitrate values greater than 1 μM are shaded. Contour interval is 2 μM. The 0.01 μM isoline is dashed. (c) Same as Figure 8b for the nitrate content at the base of the euphotic layer. (d) Surface zonal current (m s^{-1}). Eastward currents are shaded. Contour interval is 0.4 m s^{-1}. The position of the SSS front (defined as the 35.8 psu isohaline) is superimposed on all diagrams (thick dashed line). The dashed lines represent the downwelling Kelvin waves generated in December 1996 and in March 1997.

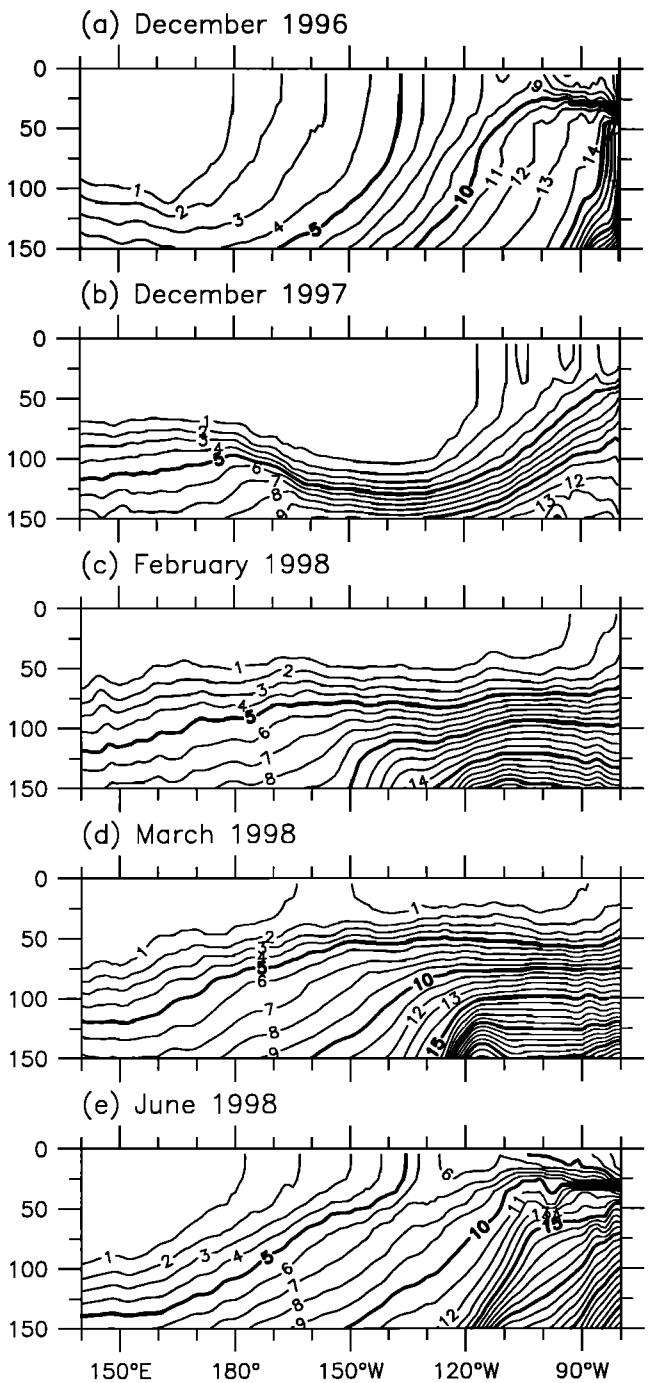

Figure 9. Vertical sections of modeled monthly mean nitrate concentration (μM) along the equator. Contour interval is 1 μM.

New production in the euphotic layer is compared to new production integrated in the upper 40 m (surface layer), and between 40 m and the bottom of the euphotic layer (subsurface layer) at 0°, 165°E (Figure 10a) and 0°, 140°W (Figure 10b).

West of the biological front, the surface layer is nitrate depleted (Figure 8b). As nitrate is the limiting nutrient in the surface layer, new production occurs largely in the subsurface layer where nitrate is available (Figure 8c) and light is still sufficient. This situation is characteristic of oligotrophic waters [*Navarette*, 1998] and results in low new production in the warm pool region (Figure 8a). In oligotrophic situations, which prevailed at 0°, 165°E in 1997 (Figure 10a) and at 0°, 140°W from November 1997 to January 1998 (Figure 10b), the nitrate uptake at the base of the euphotic layer predominantly controlled new production. In contrast, east of the front, nitrate is available from the surface down to the base of the euphotic layer (Figures 8b and 8c). New production is limited by light and micronutrients such as iron [*Barber et al.*, 1996; *Gordon et al.*, 1997] and occurs mostly in the upper region of the euphotic layer. This HNLC situation is encountered in the cold tongue at 0°, 165°E in 1998 (Figure 10a) or at 0°, 140°W throughout the period except from November 1997 through January 1998 (Figure 10b). While new production occurring below 40 m can amount to one third of the total new production, the temporal evolution of the total new production is fixed by processes taking place in the top 40 m (Figure 10b). This is not true when the nitrate-exhausted region of the western Pacific moves to the east in conjunction with El Niño. In this case, oligotrophic conditions expand eastward, and the nitrate limitation causes a collapse of the new production.

So, new production variations are controlled episodically by nitrate changes in the subsurface layer, and the variability of the new production in 1997-1998 reflects mainly changes of the nitrate uptake in the surface layer (Figure 10). Earlier studies have shown that nitrate concentrations are controlled by physical dynamics rather than biology at first order (*Loukos and Mémery* [1999] for the equatorial Atlantic; *Stoens et al.* [1999] for the equatorial Pacific). Thus we need to understand the main processes controlling the nitrate changes to understand what causes new production variations. In order to examine the temporal evolution of the nitrate budget in the euphotic layer, the nitrate tendency terms have been integrated over the surface layer and the subsurface layer. The evolution of nitrate changes, zonal and meridional advection, and vertical processes (vertical advection plus

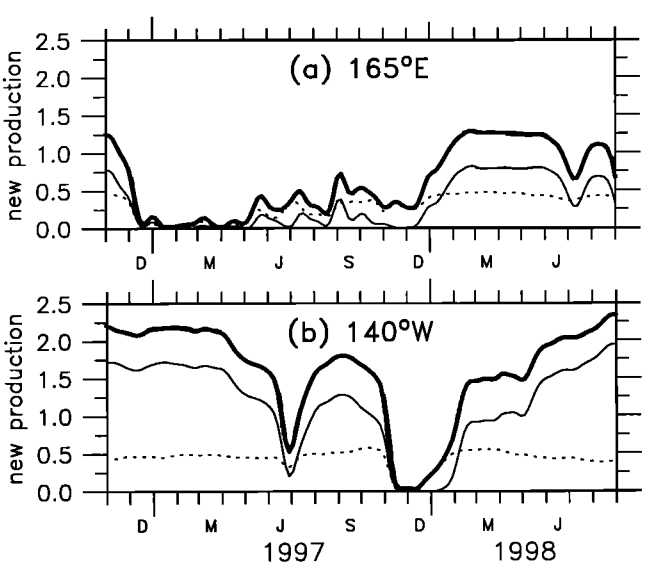

Figure 10. Time series of the modeled new production (mmol N m^{-2} d^{-1}) at (a) 165°E and (b) 140°W. The thick line is the new production in the euphotic layer, the thin line is the new production in the upper 40 m, and the dotted line is the new production between 40 m and the base of the euphotic layer. A 5° zonal moving window averaging and a seven time step (35 days) Hanning filter have been applied.

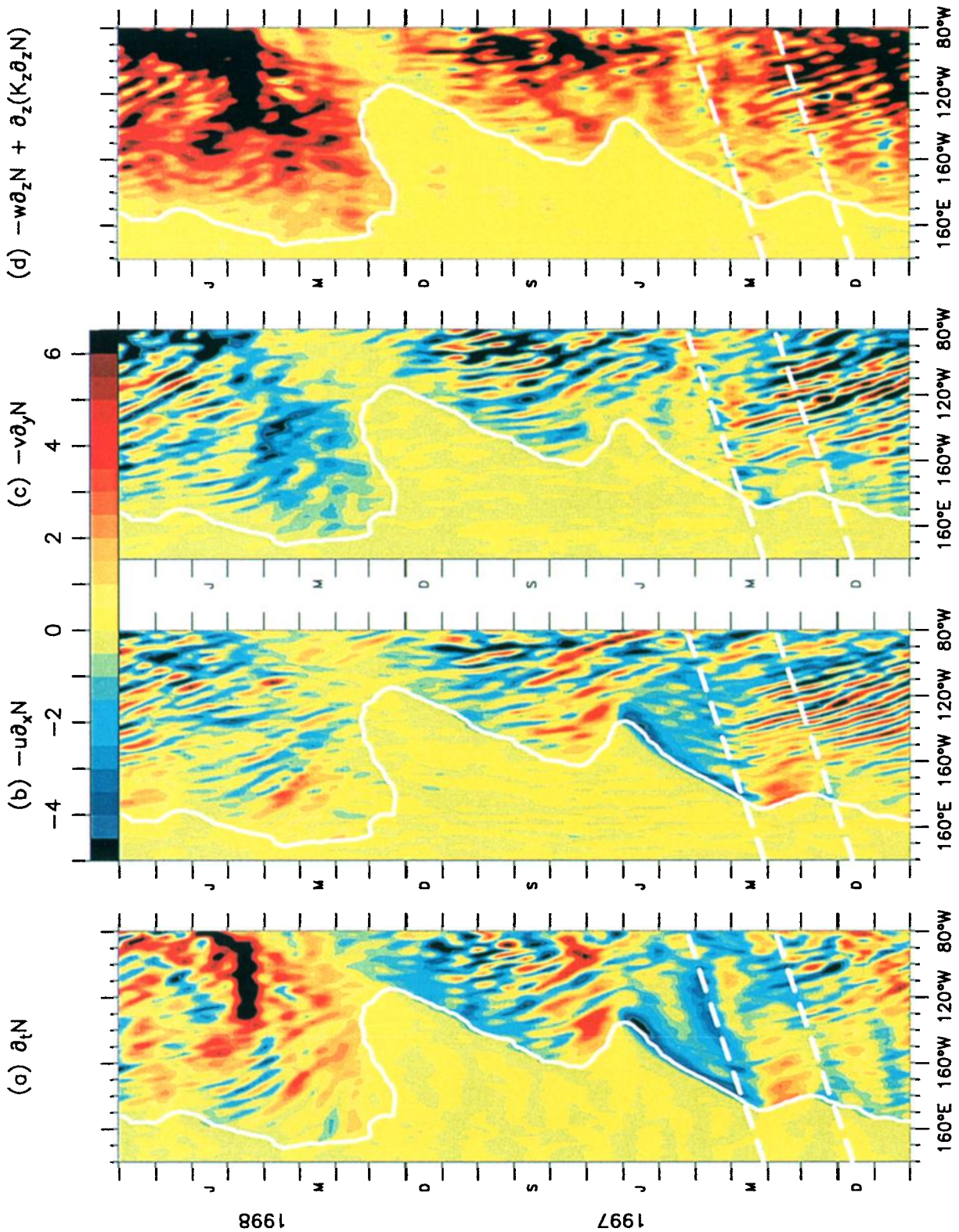

Plate 1. Time-longitude diagram of the modeled nitrate trends integrated in the upper 40 m along the equator (mmol N m^{-2} d^{-1}), showing (a) nitrate changes ($\partial_t N$); (b) zonal advection ($-u\partial_x N$); (c) meridional advection ($-v\partial_y N$); and (d) vertical processes (vertical diffusion plus vertical advection: $-w\partial_z N + \partial_z(-K_z\partial_z N)$). A 5° zonal moving window averaging and a seven time step (35 days) Hanning filter have been applied. The solid white line is the position of the new production front (defined as the 1 mmol N m^{-2} d^{-1} isoline). The dashed white lines represent the downwelling Kelvin waves generated in December 1996 and in March 1997.

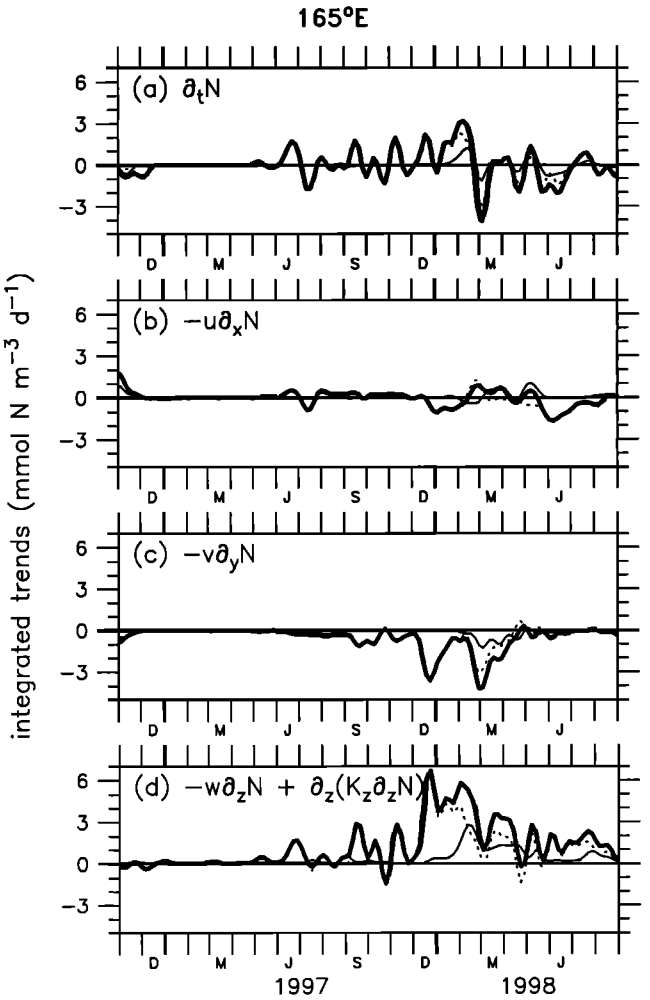

Figure 11. Time series of the nitrate trends (mmol N m^{-2} d^{-1}) at 0°, 140°W, showing (a) nitrate changes; (b) zonal advection; (c) meridional advection; and (d) vertical processes. The thick line is used for trends integrated over the euphotic layer, the thin line is for trends in the upper 40 m, and the dotted line is for trends between 40 m and the base of the euphotic layer. A 5° zonal moving window averaging and a seven time step (35 days) Hanning filter have been applied.

vertical diffusion) along the equator in the 0-40 m layer is shown in Plate 1. This provides an insight on how nitrate-limited conditions set up in the central and eastern equatorial Pacific. The vertically averaged nitrate tendencies in both layers are also shown at 140°W in Figure 11 and at 165°E in Figure 12.

The impact of physical variability on biology is greater in the cold tongue than in the warm pool as underlined by *Stoens et al.* [1999, Figure 7] during the 1992-1995 mild El Niño period. Similarly, nitrate tendencies in the surface layer during the strong 1997-1998 event (Plate 1) show two regimes controlling nitrate in the warm pool and in the upwelling region. Weak nitrate tendencies appear west of the convergence front, whereas the upwelling region is characterized by more active physical processes that take place at different timescales and space scales. For instance, the effect of the westward propagating instability waves on the nitrate budget can be seen in the zonal and meridional advection terms, as well as in the vertical processes (Plate 1 and Figure 11). They are active before March 1997 and extend as far west as 170°W after March 1998 [*Chavez et al.*, 1999, Figure 5] with the return of La Niña conditions (Figure 8d). Their activity is diminished in-between as expected during an El Niño period [*Philander et al.*, 1985]. These waves have complex three-dimensional patterns [*Vialard et al.*, 2001; *Kennan and Flament*, 2000; also C. Menkes et al., A whirling ecosystem in the equatorial Atlantic, submitted to *Nature*, 2001] that act to redistribute nitrate, plankton, heat, and salt. Specific studies considering their three-dimensional structure must be done before drawing conclusions about their exact role in these different budgets at seasonal timescales.

Eastward propagating Kelvin waves also have a clear impact on the nitrate budget. Three processes explain the decrease of surface nitrates associated with the downwelling Kelvin waves such as those of December 1996 and March 1997 (Plate 1a). First, downwelling Kelvin waves produce associated eastward currents that advect nutrient-poor waters from the western Pacific eastward (Plate 1b). Second, the deepening of the nitracline related to the downwelling wave may induce a reduction of the supply of nitrate-rich waters in the surface layer. Third, the mean upwelling vertical velocity is reduced along the track of the wave, leading to a decrease of the vertical advection of nitrate-rich waters (Plate 1d). These processes only act efficiently east of the front. West of the front, they are weaker because the nitracline is very deep (Figure 9a) and horizontal advection is weak (Plate 1 and

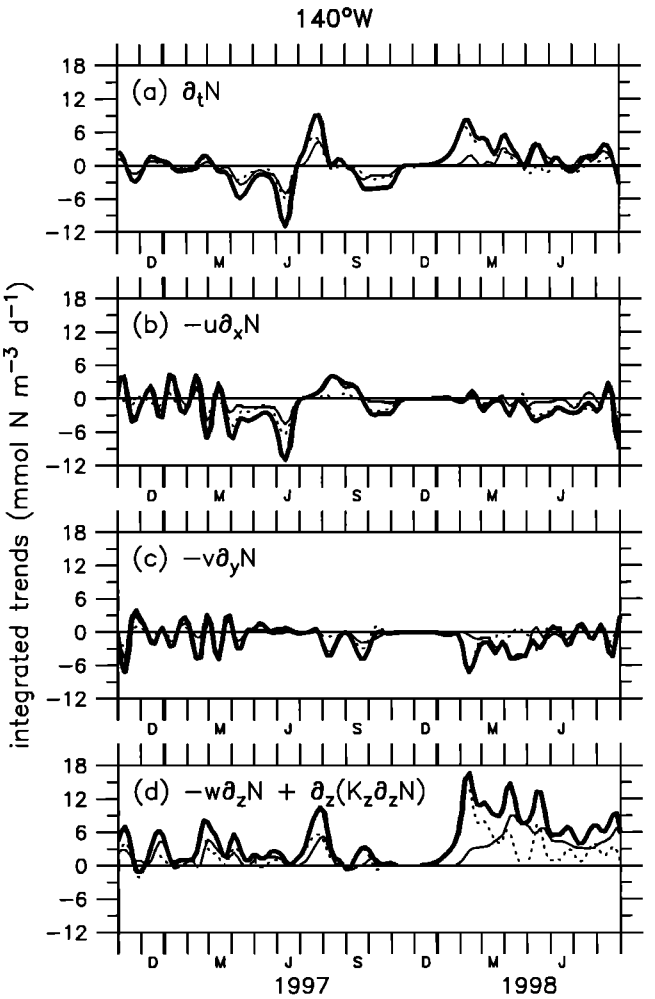

Figure 12. Same as Figure 11 for 0°, 165°E.

Figure 12) since horizontal nitrate gradients are weak (Figure 8b). Finally, a weak vertical diffusion (well-mixed surface layer; Figure 9a) together with weak vertical velocity leads to weak vertical processes (Plate 1 and Figure 12).

The consequence of the first Kelvin wave (forced in December 1996) is a small eastward movement of the biological front (indicated by a thick white line in Plate 1) associated with the displacement of the salinity front. It quickly ends as westerly winds (Figure 5a), and thus eastward currents (Figure 8d) stop. Then, a patch of westward currents (Figure 8d) appears when easterlies strengthen (Figure 5a). At that time, westward advection and upwelling of nitrate-rich waters resume for a short period (Plates 1b and 1d) and lead to a small westward shift of the front (January-February 1997). The downwelling Kelvin wave associated with the second westerly wind burst (March 1997) initiates a more powerful eastward displacement of the front. During its eastward motion, the frontal region experiences a strong zonal convergence under the action of the eastward flowing surface current from the west (Figure 8d) associated with the eastward moving westerlies (Figure 5a) [*Vialard et al.*, 2001]. The nitrate zonal gradient strengthens (Figure 8b) and a strong negative zonal advection takes place (Plate 1b). In late June 1997, nutrient-poor waters of the warm pool reach 140°W. Both zonal advection (Plate 1b) and reduced vertical supply (Plate 1d) drive the nitrate impoverishment at that location. As a result, the surface layer is nitrate exhausted in the central Pacific (Figure 8b) and new production is greatly reduced in the surface layer (Figure 10).

In July 1997, the biological front retreats westward by about 20°. This is the result of westward advection of nitrate-rich waters (Plate 1b) from the east in association with the seasonal strengthening of the trades (Figure 5a). Besides, the vertical supply of nitrate-rich waters from below is increased (Plate 1d and Figure 11d). More precisely, nitrate is advected upward from the nutricline (the base of the euphotic zone), and then, it is redistributed in the surface layer via vertical diffusion. Thus both the westward advection of nutrient-rich waters (Plate 1b and Figure 11b) and nitrate supply from the subsurface (Plate 1d and Figure 11d) contribute to the nitrate replenishment of the upper layer. During that short period, the new production increases in the upper 40 m in the central Pacific (Figure 10b).

The westward expansion of the nutrient-rich waters of the cold tongue stops when large-scale westerly winds develop in the central Pacific, and start driving the warm pool eastward again. During the second half of 1997, a sustained decrease of nitrate occurs everywhere east of the biological front (Plate 1a) because the vertical supply has decreased (the nitrate-rich pool is deep in the central equatorial Pacific; Figure 9b), and cannot overcome losses through horizontal processes (Plate 1). At 140°W, the passage of the front (negative zonal advection in October 1997 in Figure 11b) is followed by a period with no advective processes (Figure 11) that lasts about 1.5 months. At that time, conditions in the central Pacific are those usually found in the warm pool, and the euphotic layer is completely nitrate depleted.

During the mature phase of El Niño in the western Pacific, the nutricline is uplifted (Figure 9b) compared to its normal value (Figure 9a). Nitrate is brought to the lower layer of the euphotic zone (Figure 8c) through vertical processes (Figure 12). During that period, new production occurs essentially in the subsurface layer (Figure 10a).

At the end of 1997, mesotrophic conditions prevail west of the date line, while poor conditions still prevail in the eastern part of the basin. At that time, in the western Pacific, the westerly wind anomaly has turned into an easterly anomaly (Figure 5a) and the nitracline is lifted (Figure 9c). The nitrate inputs driven by vertical mechanisms reach the surface layer (Figure 12d). This process intensifies in early 1998, and new production increases in the western Pacific. The same process then appears in the central Pacific as the nitracline shoaling propagates eastward. A sustained vertical nitrate supply at the base of the euphotic layer overcomes losses through meridional advection and leads to an increase of new production in January 1998 (Figure 11). Nitrate changes in the surface layer occur about 1 month later driven by vertical input (Plate 1 and Figure 11).

In March 1998, the basin-wide nitracline east-west slope begins to set up again (Figure 9d). As the nitracline starts to deepen at 165°E, nitrate upward transport by vertical processes decreases and is overcome again by horizontal nitrate losses (Figure 12). In the central Pacific, the intensification of easterly winds boosts the local upwelling (Figure 9d) and leads to stronger nitrate vertical supply than meridional losses (Figure 11).

In May 1998, westerly wind anomalies disappear in the eastern Pacific and trade winds recover in the entire equatorial region (Figure 5a). Easterlies, together with a shallow nitracline, produce a very efficient upwelling that brings more nitrate into the surface layer. During this period, vertical nitrate supply from the deeper layer to the upper layer of the euphotic zone is the strongest (Figure 11). At that time, cold and rich conditions resume in the central Pacific, and the mesotrophic conditions extend further west than 165°E during several months.

6. Discussion and Conclusion

Our objective was to analyze the interannual variability of new production in relation to the variability of the physical parameters in the equatorial Pacific during a major El Niño event. In particular, a primary point of this study was to understand how the central Pacific became nitrate depleted during the mature phase of the severe 1997-1998 El Niño, as reported by *Chavez et al.* [1999]. To that end, we combined available observations and results of a physical and biogeochemical model into a synthetic view of the processes during this period. A general circulation model forced with remotely sensed wind stress was used to drive a nitrate transport model.

Despite an overall agreement between our simulation and available nitrate and new production observations, some problems are still apparent. The vertical stratification of the physical simulation is too diffuse in the thermocline zone [*Vialard et al.*, 2001]. This may lead to a too diffuse nitracline. For instance, after the 8-year spin up (see the model description section), the 5 μM isopleth is found at 150 m depth in the western equatorial basin instead of 100 m in the Levitus climatology. In fact, in the 1993-1998 outputs of the model (not shown), the excess in vertical diffusion is compensated by abnormally low nitrate concentrations below the pycnocline, resulting in new production estimates that are comparable with the field measurements. Another anomaly generated by the model is the strong increase in nitrate concentration (up to 40 μM) at the equator in the eastern

Pacific below 200 m. This nutrient trapping [*Najjar et al.*, 1992; *Aumont et al.*, 1999] is the result of the instantaneous remineralization of high new production below the euphotic layer, combined with weak currents at depth. It is probably responsible for abnormally high vertical flux of nitrate through upwelling and may explain why the 1993-1998 mean surface nitrate concentrations are higher in the model than in observations in the eastern Pacific (Figure 1).

During the 1997-1998 period, the growth and decay of the El Niño conditions in the ocean circulation model are remarkably in phase with observations. The scarce nitrate and new production measurements, as well as the satellite-derived chlorophyll during this period, however, suggest that the variability of the simulated biological fields is underestimated. Nevertheless, the chronology of the extension and of the retreat of the modeled oligotrophic waters of the fresh warm pool is qualitatively in agreement with ocean color data. Thus our model appears to be a suitable tool to study the evolution of nitrate and new production fields induced by physical ocean dynamics associated with the El Niño event. The model agrees with observations [*Kuroda and McPhaden*, 1993; *Eldin et al.*, 1997] showing that the eastern edge of the fresh warm pool separates western oligotrophic waters from richer upwelled waters in the east (Figure 8). The response of nitrate to environmental processes occurs at different timescales and space scales on each side of the front. In the warm pool, the variability is essentially intraseasonal in response to the wind burst variability or interannual in response to ENSO variability. In the cold tongue, the variability is observed at interannual and annual scales, and the intraseasonal signal includes a strong signal from the tropical instability waves and from the Kelvin waves. In particular, during El Niño, the latter waves are essentially downwelling in response to the westerly wind activity in the western Pacific. These waves induce an eastward advection of nitrate-poor waters from the western basin, a depression of the nutricline, and a reduction of the vertical velocity that lead to a decrease of the nitrate concentration in the euphotic layer. Their impact is of primary importance in simulating the nutrient-poor conditions resulting from the 1997 El Niño.

The first phase that begins in late 1996 is a growth phase of El Niño. Strong westerly wind bursts in the western Pacific advect eastward the nitrate-poor waters of the warm pool. The deepening of the nitracline starts to propagate eastward, and the vertical nitrate supply is greatly reduced. This phase ends in June 1997 as the nutrient-poor waters reach 140°W. The second phase is a short cessation of the invasion of nitrate-poor waters. Because of a short-lived increase of the easterlies in the eastern Pacific, westward advection of nitrate-rich waters from the east and a vertical supply increase result in a slight retreat of the biological front to the west. The third phase is the mature phase (November 1997 through January 1998), when nitrate-poor waters extend over most of the equatorial Pacific. Two processes act to maintain the biologically poor conditions during that period: Nitrate-poor water from the warm pool is advected toward the central Pacific, and the nitrate vertical input is suppressed as the nitracline deepens in the east. In contrast to the moderate 1991-1992 El Niño when nitrate persisted at the surface [*McCarthy et al.*, 1996], no nitrate is measured in the surface layer in the central Pacific [*Chavez et al.*, 1999] in 1997. This situation, accurately simulated, lasted from June 1997 to February 1998. The nitracline (Figure 9b) and thermocline (not shown) are shallower in the western Pacific than in the central Pacific. Consequently, nitrate is available at shallower depths in the western Pacific than in the central Pacific. The euphotic layer of the central Pacific is nitrate depleted, and new production is lower than in the western Pacific. During several months, the central Pacific experiences warm pool oligotrophic conditions (Figure 8). Such a duration is reminiscent of the intense 1982-1983 El Niño when a low-nitrate condition was estimated to last more than 6 months [*Barber and Kogelschatz*, 1990]. In January 1998, modeled new production in the *Wyrtki* [1981] box is estimated to be lower by 40% compared to the mean 1993-1996 value. During the fourth phase (early 1998), the nitracline becomes shallow over most of the basin, preparing for the recovery of nitrate-rich conditions. So, efficient nitrate vertical supply over a large part of the equatorial Pacific triggers the return of high biological production conditions when trade winds strengthen in May 1998. Then, cold and nitrate-rich conditions extend far into the western Pacific during the La Niña phase.

In the western Pacific, vertical processes in the subsurface layer account for a great part of the nitrate variations in the euphotic layer. During the mature phase, vertical nitrate input associated with the uplifting of the nutricline in the western Pacific increases the nitrate content at the base of the euphotic layer. It is also vertical processes that drive the onset and maintenance of nitrate-rich conditions associated with La Niña.

During this 6 year experiment, the modeled eastern edge of the warm pool (commonly taken as the 29°C isotherm) coincides with a salinity-nitrate front, except when warm waters invade the entire equatorial Pacific in January-March 1998. At that time, the salinity-biology front moves from the eastern edge of the warm pool (not shown). However, observations and results of a recent modeling study including interannual variability of precipitation show that the freshening invaded the whole Pacific at the El Niño peak (J. Vialard et al., submitted manuscript, 2001), as did warm waters. Similarly, a stronger nitrate decrease would have probably been achieved in the euphotic layer of the entire equatorial Pacific by using a model with more realistic vertical nitrate fluxes. At least, the location and intensity of the modeled biological front would be different.

The extension of the nutrient-rich waters far in the west associated with La Niña conditions in 1998 is correctly reproduced in the model. Nevertheless, the swift return of rich conditions in 1998 is underestimated, both in terms of nitrate concentration (comparison with measurements in June 1998 [*Strutton and Chavez*; 2000]) and in terms of new production. The simulated equatorial chlorophyll increase is less intense than the one detected from the ocean color satellite. Also, the small-scale chlorophyll bloom at 165°E is not reproduced. Actually, the thermocline (modeled or observed) and nitracline were uplifted to about 40 m in this region in February-June 1998 because of a local upwelling driven by easterly wind anomalies that prevailed in the western Pacific [*Murtugudde et al.*, 1999]. Yet, the response of the biological model to the environmental changes was very weak. Indeed, all the analysis in this paper is concerned with the variations of one single nutrient, and the failure to simulate blooms shows the limitations of the simple nitrate model in cases of abnormally high chlorophyll concentration. This failure can possibly be attributed to the lack of iron input [*Chavez et al.*,

1999] in our model. Considering that the EUC is the main source of iron for the euphotic layer [*Barber et al.*, 1996; *Gordon et al.*, 1997], the shoaling (depression) of the EUC, which is accurately reproduced, would drive an increase (decrease) of the iron vertical flux at the ENSO timescale, but also at the timescale of mesoscale processes such as instability waves [*Friedrichs and Hofmann*, 2001]. Therefore adding a limitation by iron should intensify the link between the physical dynamics and biological production, and would certainly enhance the variability of the new production in the central equatorial Pacific, as shown by *Loukos et al.* [1997]. Another cause of the observed bloom in 1998 could be the lack of herbivores [*Leonard and McClain*, 1996]. It is reasonable to think that following the phytoplankton waning during El Niño, the zooplankton population has greatly diminished. At that time, the relaxation of the grazing pressure could be one of the processes responsible for the remarkable biomass increase because generation timescales for zooplankton are greater than those for phytoplankton. The chlorophyll-nitrate statistical relationship [*Stoens et al.*, 1999] used in the biogeochemical model is established for the HNLC conditions that usually prevail in the equatorial Pacific. Thus it cannot properly represent bloom conditions.

In the equatorial western region, blooms have already been observed with the Coastal Zone Color Scanner (CZCS), in particular in December 1981 (C. Dupouy, personal communication, 2001). The remote sensing estimation of the chlorophyll concentration of these blooms may be distorted because of the possible dominance of strongly absorbing species such as *Synechococcus* [*Morel*, 1997] or that of tropical phytoplankton observed at 20°S [*Dupouy et al.*, 2000].

Besides the insight into processes allowed by this study, we must point out the difficulty in validating the model results with chemical or biological data. Despite ocean color that provides high-quality data, there is a lack of in situ data to validate modeled biological fields. Adding biogeochemical sensors to moorings would provide vertical structure information, of benefit to biological models.

Acknowledgments. We thank the TOGA-TAO Project Office directed by M. J. McPhaden for sharing the time series data from the mooring array. We also thank the chief scientists and data managers of the WOCE and JGOFS international programs, who made their data available. We acknowledge D. Mackey and CSIRO for sharing unpublished nitrate data on the warm pool, and F. Chavez, who gave us his historical data set. Very helpful discussions with L. Mémery were greatly appreciated.

References

Aumont, O., J. C. Orr, P. Monfray, G. Madec, and E. Maier-Reimer, Nutrient trapping in the equatorial Pacific: The ocean circulation solution, *Global Biogeochem. Cycles*, 13, 351-369, 1999.

Barber, R. T., and F. P. Chavez, Biological consequences of El Niño, *Science*, 222, 1203-1210, 1983.

Barber, R. T., and J. E. Kogelschatz, Nutrients and productivity during the 1982/83 El Niño, in *Global Ecological Consequences of the 1982-83 El Niño-Southern Oscillation*, edited by P. W. Glynn, pp. 21-53, Elsevier, New York, 1990.

Barber, R. T., M. P. Sanderson, S. T. Lindley, F. Chai, J. Newton, C. C. Trees, D. G. Foley, and F. P. Chavez, Primary productivity and its regulation in the equatorial Pacific during and following the 1991-1992 El Niño, *Deep Sea Res., Part II*, 43, 933-969, 1996.

Baturin, N. G., and P. P. Niiler, Effects of instability waves in the mixed layer of the equatorial Pacific, *J. Geophys. Res.*, 102, 27,771-27,793, 1997.

Bentamy, A., Y. Quilfen, N. Grima, F. Gohin, M. Lenaour, and J. Servain, Determination and validation of average wind fields from ERS-1 scatterometer measurements, *Global Atmos. Ocean Syst.*, 4, 1-29, 1996.

Blanke, B., and P. Delecluse, Variability of the tropical Atlantic Ocean simulated by a general circulation model with two different mixed layer physics, *J. Phys. Oceanogr.*, 23, 1363-1388, 1993.

Boulanger, J.-P., and C. Menkes, Long equatorial wave reflection in the Pacific Ocean from TOPEX/Poseidon during the 1992-1998 period, *Clim. Dyn.*, 15, 205-225, 1999.

Boutin, J., et al., Satellite sea surface temperature: A powerful tool for interpreting in situ pCO_2 measurements in the equatorial Pacific Ocean, *Tellus Ser. B*, 51, 490-508, 1999.

Carr, M. E., M. R. Lewis, D. Kelly, and B. Jones, A physical estimate of new production in the equatorial Pacific along 150°W, *Limnol. Oceanogr.*, 40, 138-147, 1995.

Chai, F., S. T. Lindley, and R. T. Barber, Origin and maintenance of high nitrate condition in the equatorial Pacific, *Deep Sea Res., Part II*, 43, 1031-1064, 1996.

Charney, J. G., and S. L. Spiegel, Structure of wind-driven equatorial currents in homogeneous oceans, *J. Phys. Oceanogr.*, 1, 149-160, 1971.

Chavez, F. P., K. R. Buck, S. K. Service, J. Newton, and R. T. Barber, Phytoplankton variability in the central and eastern tropical Pacific, *Deep Sea Res., Part II*, 43, 835-870, 1996a.

Chavez, F. P., S. K. Service, and S. E. Buttrey, Temperature-nitrate relationships in the central and eastern tropical Pacific, *J. Geophys. Res.*, 101, 20,553-20,563, 1996b.

Chavez, F. P., P. G. Strutton, and M. J. McPhaden, Biological-physical coupling in the central Pacific during the onset of the 1997-98 El Niño, *Geophys. Res. Lett.*, 25, 3543-3546, 1998.

Chavez, F. P., P. G. Strutton, G. E. Friederich, R. A. Feely, G. C. Feldman, D. G. Foley, and M. J. McPhaden, Biological and chemical response of the equatorial Pacific Ocean to the 1997-98 El Niño, *Science*, 286, 2126-2131, 1999.

Conkright, M. E., S. Levitus, and T. P. Boyer, *World Ocean Atlas 1994*, vol. 1, Nutrients, *NOAA Atlas NESDIS 1*, 150 pp., U.S. Dep. of Commer., Washington, D.C., 1994

Cromwell, T. S., Circulation in a meridional plane in the central equatorial Pacific, *J. Mar. Res.*, 12, 196-213, 1953.

Dandonneau, Y,. Monitoring the sea surface chlorophyll concentration in the tropical Pacific: Consequences of the 1982-83 El Niño, *Fish. Bull.*, 84, 687-695, 1986.

Dandonneau, Y., Surface chlorophyll concentration in the tropical Pacific Ocean: An analysis of data collected by merchant ships from 1978 to 1989, *J. Geophys. Res.*, 97, 3581-3591, 1992.

Dandonneau, Y., Introduction to special section: Biogeochemical conditions in the equatorial Pacific in late 1994, *J. Geophys. Res.*, 104, 3291-3295, 1999.

Delcroix, T., Observed surface oceanic and atmospheric variability in the tropical Pacific at seasonal and ENSO timescales: A tentative overview, *J. Geophys. Res.*, 103, 18,611-18,633, 1998.

Delcroix, T., G. Eldin, M. H. Radenac, J. Toole and E. Firing, Variation of the western equatorial Pacific Ocean, 1986-1988, *J. Geophys. Res.*, 97, 5423-5445, 1992.

Delcroix, T., C. Hénin, V. Porte, and P. Arkin, Precipitation and sea-surface salinity in tropical Pacific, *Deep Sea Res., Part I*, 43, 1123-1141, 1996.

Delcroix, T., and J. Picaut, Zonal displacement of the western equatorial Pacific fresh pool, *J. Geophys. Res.*, 103, 1087-1098, 1998.

Delcroix, T., L. Gourdeau, and C. Hénin, Sea surface salinity changes along the Fiji-Japan shipping track during the 1996 La Niña and 1997 El Niño period, *Geophys. Res. Lett.*, 25, 3169-3172, 1998.

Deschamps, P. Y., F. M. Breon, M. Leroy, A. Podaire, A. Bricaud, J. C. Buriez, and G. Seze, The POLDER mission: Instrument characteristics and scientific objectives, *IEEE Trans. Geosci. Remote Sens.*, 32, 598-615, 1994.

Dugdale, R. C., F. P. Wilkerson, R. T. Barber and F. P. Chavez, Estimating new production in the equatorial Pacific Ocean at 150°W. *J. Geophys. Res.*, 97, 681-686, 1992.

Dupouy-Douchement, C., H. Oiry, A. Le Bouteiller, and M. Rodier, Variability of the equatorial phytoplankton enrichment as followed by CZCS in the western and central equatorial Pacific Ocean during 1981 and 1982, in *Remote Sensing of the Ocean*,

edited by S. F. Jones, et al., pp. 406-419, Seibutsu Kenkyusha, Tokyo, 1993.

Dupouy, C., J. Neveux, A. Subramaniam, M. R. Mulholland, J. P. Montoya, L. Campbell, E. J. Carpenter, and D. G. Capone, Satellite captures *Trichodesmium* blooms in the southwestern tropical Pacific, *Eos, Trans. AGU*, 81, 13, 2000.

Eldin, G., M. Rodier, and M. H. Radenac, Physical and nutrient variability in the upper equatorial Pacific associated with westerly wind forcing and wave activity in October 1994, *Deep Sea Res., Part II*, 44, 1783-1800, 1997.

Foley, D. G., D. Dickey, M. J. McPhaden, R. R. Bidigare, M. R. Lewis, R. T. Barber, S. Lindley, C. Garside, D. V. Manov, and J. D. McNeil, Longwaves and primary productivity variations in the equatorial Pacific at 0°, 140°W, *Deep Sea Res., Part II*, 44, 1801-1826, 1997.

Friedrichs, M. A. M., and E. E. Hofmann, Physical control of biological processes in the central equatorial Pacific Ocean, *Deep Sea Res., Part I*, 48, 1023-1069, 2001.

Fu, L.-L., E. J. Christensen, C. A. Yamarone Jr., M. Lefebvre, Y. Ménard, M. Dorrer, and P. Escudier, TOPEX/Poseidon mission overview, *J. Geophys. Res.*, 99, 24,369-24,381, 1994.

Gibson, R., P. Kallberg, S. Uppala, A. Hernandez, A. Nomura, and K E. Serrano, The ECMWF re-analysis project report series, 1, ERA description, technical report, Eur. Cent. For Medium-Range Weather Forecasts, Reading, England, 1997.

Gordon, R. M., K. H. Coale, and K. S. Johnson, Iron distribution in the equatorial Pacific: Implications for new production, *Limnol. Oceanogr.*, 43, 419-431, 1997.

Grima, N., A. Bentamy, K. Katsaros, Y. Quilfen, P. Delecluse, and C. Lévy, Sensitivity of an oceanic general circulation model forced by satellite wind-stress fields, *J. Geophys. Res.*, 104, 7967-7989, 1999.

Halpern, D., and G. C. Feldman, Annual and interannual variations of phytoplankton pigment concentration and upwelling along the Pacific equator, *J. Geophys. Res.*, 99, 7347-7354, 1994.

Hayes, S. P., L. J. Mangum, J. Picaut, A. Sumi, and K. Takeuchi, TOGA-TAO: A moored array for real-time measurements in the tropical Pacific Ocean, *Bull. Am. Meteorol. Soc.*, 72, 339-347, 1991.

Honjo, S., Sedimentation of material in the Sargasso Sea at 5,367 m, *J. Mar. Res.*, 36, 469-492, 1978.

Inoue, H. Y., M. Ishii, H. Matsueda, and M. Ahoyama, Changes in longitudinal distribution of the partial pressure of CO_2 (pCO_2) in the central and western equatorial Pacific, west of 160°W, *Geophys. Res. Lett.*, 14, 1781-1784, 1996.

Kennan, S. C., and P. Flament, Observations of a tropical instability vortex, *J. Phys. Oceanogr.*, 30, 2277-2301, 2000.

Kessler, W. S., M. J. McPhaden, and K. M. Weickmann, Forcing of intraseasonal Kelvin waves in the equatorial Pacific, *J. Geophys. Res.*, 100, 10,613-10,631, 1995.

Kessler, W. S., M. C. Spillane, M. J. McPhaden, and D. E. Harrison, Scales of variability in the equatorial Pacific inferred from the Tropical Atmosphere Ocean (TAO) buoy array, *J. Clim.*, 9, 2999-3024, 1996.

Kuroda, Y., and M. J. McPhaden, Variability in the western equatorial Pacific Ocean during Japanese Pacific Climate Study Cruises in 1989 and 1990, *J. Geophys. Res.*, 98, 4747-4759, 1993.

Landry, M. R., et al., Iron and grazing constraints on primary production in the central equatorial Pacific: An EqPac synthesis, *Limnol. Oceanogr.*, 42, 405-418, 1997.

Le Borgne, R,. and M. Rodier, Net zooplankton and the biological pump: A comparison between the oligotrophic and mesotrophic equatorial Pacific, *Deep Sea Res., Part II*, 44, 2003-2023, 1997.

Le Borgne, R., M. Rodier, A. Le Bouteiller, and J. W. Murray, Zonal variability of plankton and particle export flux in the equatorial Pacific upwelling between 165°E and 150°W, *Oceanol. Acta*, 22, 57-66, 1999.

Leonard, C. L., and C. R. McClain, Assessment of interannual variation (1979-1986) in pigment concentrations in the tropical Pacific using the CZCS, *Int. J. Remote Sens.*, 17, 721-732, 1996.

Levitus, S., Climatological atlas of the world ocean, NOAA Professional Paper No 13, 173 pp, U.S. Gov. Print. Off., Washington, D.C., 1982.

Loukos, H., and L. Mémery, Simulation of the nitrate seasonal cycle in the equatorial Atlantic Ocean during 1983 and 1984, *J. Geophys. Res.*, 104, 15549-15573, 1999.

Loukos, H., B. Frost, D. E. Harrison, and J. W. Murray, Ecosystem model with iron limitation of primary production in the equatorial Pacific at 140°W, *Deep Sea Res., Part II*, 44, 2221-2249, 1997.

Mackey, D. J., J. Parslow, F. B. Griffiths, H. W. Higgins, and B. Tilbrook, Plankton productivity and the carbon cycle in the western equatorial Pacific under ENSO and non-ENSO conditions, *Deep Sea Res., Part II*, 44, 1951-1978, 1997.

McCarthy, J. J., C. Garside, J. L. Nevins, and R. T. Barber, New production along 140°W in the equatorial Pacific during and following the 1992 El Niño event, *Deep Sea Res., Part II*, 43, 1065-1093, 1996.

McCarty, M. E,. and M. J. McPhaden, Mean seasonal cycles and interannual variations at 0°, 165°E during 1986-1992, *NOAA Tech. Memo. ERL PMEL-98*, 64 pp., 1993

McPhaden, M. J., Genesis and evolution of the 1997-98 El Niño, *Science*, 283, 950-954, 1999.

McPhaden, M. J., and S. P. Hayes, Variability in the eastern equatorial Pacific during 1986-1988, *J. Geophys. Res.*, 95, 13,195-13,208, 1990.

McPhaden, M. J., et al., The Tropical Ocean-Global Atmosphere observing system: A decade of progress, *J. Geophys. Res.*, 103, 14,169-14,240, 1998.

Minas, H. J., M. Minas, and T.T. Packard, Productivity in upwelling areas deduced from hydrographic and chemical fields, *Limnol. Oceanogr.*, 31, 1182-1206, 1986.

Morel, A., Consequences of a *Synechococcus* bloom upon the optical properties of oceanic (case 1) waters, *Limnol. Oceanogr.*, 42, 1746-1754, 1997.

Morel, A., and J.-F. Berthon, Surface pigments, algal biomass profiles, and potential production of the euphotic layer: Relationships investigated in view of remote-sensing applications, *Limnol. Oceanogr.*, 34, 1545-1562, 1989.

Murray, J. W., R. T. Barber, M. R. Roman, M. P. Bacon, and R. A. Feely, Physical and biological controls on carbon cycling in the equatorial Pacific, *Science*, 266, 58-65, 1994.

Murtugudde, R. G., S. R. Signorini, J. R. Christian, A. J. Busalacchi, C. R. McClain, and J. Picaut, Ocean color variability of the tropical Indo-Pacific basin observed by SeaWiFS during 1997-98, *J. Geophys. Res.*, 104, 18,351-18,365, 1999.

Najjar, R. G., J. L. Sarmiento, and J. R. Toggweiler, Downward transport and fate of organic matter in the ocean: Simulation with a general circulation model, *Global Biogeochem. Cycles*, 6, 45-76, 1992.

Navarette, C., Dynamique du phytoplancton en océan équatorial: Mesures cytométriques et mesures isotopiques durant la campagne FLUPAC, en octobre 1994 dans la partie ouest du Pacifique, thèse de doctorat, 313 pp, Univ. Paris VI, Paris, 1998.

Neelin, J. D., D. S. Battisti, A. C. Hirst, F.-F. Jin, Y. Wakata, T. Yamagata, and S. E. Zebiak, ENSO theory, *J. Geophys. Res.*, 103, 14,261-14,290, 1998.

O'Reilly, J. E., S. Maritorena, B. G. Mitchell, D. A. Siegel, K. L. Carder, S. A. Garver, M. Kahru, and C. McClain, Ocean color chlorophyll algorithms for SeaWiFS, *J. Geophys. Res.*, 103, 24,937-24,953, 1998.

Peña, M. A., W. G. Harrison, and M. R. Lewis, New production in the central equatorial Pacific, *Marine Ecology Progress Series*, 80, 265-274, 1992.

Peña, M. A., M. R. Lewis, and J. Cullen, New production in the warm waters of the tropical Pacific Ocean, *J. Geophys. Res.*, 99, 14,255-14,268, 1994.

Philander, S. G. H., D. Halpern, D. Hansen, R. Legeckis, L. Miller, C. Paul, R. Watts, R. Weisberg, and M. Winbush, Long waves in the equatorial Pacific Ocean, *Eos Trans. AGU*, 66, 154, 1985.

Picaut, J., M. Ioualalen, C. Menkes, T. Delcroix, and M. J. McPhaden, Mechanisms of the zonal displacements of the Pacific warm pool: implications for ENSO, *Science*, 274, 1486-1489, 1996.

Radenac, M.-H., and M. Rodier, Nitrate and chlorophyll distributions in relation to thermohaline and current structures in the western tropical Pacific during 1985-1989, *Deep Sea Res., Part II*, 43, 725-752, 1996.

Raimbault, P., G. Slawyk, B. Boudjellal, C. Coatanoan, P. Conan, B. Coste, N. Garcia, T. Moutin, and M. Pujo-Pay, Carbon and nitrogen uptake and export in the equatorial Pacific at 150°W: Evidence of an efficient regenerated production cycle, *J. Geophys. Res.*, 104, 3341-3356, 1999.

Reverdin, G., A. Morlière, and G. Eldin, ALIZÉ 2: Campagne océanographique trans-Pacifique (janvier-mars 1991): Recueil des données, *Rapp. Interne LODYC 91/13*, 341 pp, Univ. Pierre et Marie Curie, Paris, Oct. 1991, 1991.

Reverdin, G., C. Frankignoul, E. Kestenare, and M. J. McPhaden, Seasonal variability in the surface currents of the equatorial Pacific, *J. Geophys. Res.*, 99, 20,323-20,344, 1994.

Reynolds, R. W., and T. M. Smith, Improved global sea surface temperature analyses using optimum interpolation, *J. Clim.*, 7, 929-948, 1994.

Stoens, A., Étude de la variabilité du système couplé physique-biogéochimique dans le Pacifique tropical entre les années 1992 et 1995, thèse de doctorat, 223 pp, Univ. Paris VI, Paris, 1998.

Stoens, A., et al., The coupled physical-new production system in the equatorial Pacific during the 1992-1995 El Niño, *J. Geophys. Res.*, 104, 3323-3339, 1999.

Strutton, P. G., and F. P. Chavez, Primary productivity in the equatorial Pacific during the 1997-98 El Niño, *J. Geophys. Res.*, 105, 26,089-26,101, 2000.

Tapley, B. D., D. P. Chambers, C. K. Shum, R. J. Eanes, and J. C. Ries, Accuracy assessment of the large-scale dynamic ocean topography from TOPEX/Poseidon altimetry, *J. Geophys. Res.*, 99, 24,605-24,617, 1994.

Toggweiler, J. R., and S. Carson, What are upwelling systems contributing to the ocean's carbon and nutrient budgets?, in *Upwelling in the Ocean: Modern Processes and Ancient Records*, edited by C. P. Summerhayes et al., pp. 337-360, John Wiley, New York, 1995.

Vialard, J., and P. Delecluse, An OGCM study for the TOGA decade, II, Barrier layer formation and variability, *J. Phys. Oceanogr.*, 28, 1089-1106, 1998.

Vialard, J., C. Menkes, J.-P. Boulanger, P. Delecluse; E. Guilyardi, M. J. McPhaden, and G. Madec, A model study of oceanic mechanisms affecting equatorial Pacific sea surface temperature during the 1997-98 El Niño, *J. Phys. Oceanogr.*, 31, 1649-1675, 2001.

Wyrtki, K., An estimate of equatorial upwelling in the Pacific, *J. Phys. Oceanogr.*, 11, 1205-1214, 1981.

Wyrtki, K., and B. Kilonsky, Mean water and current structure during the Hawaii to Tahiti shuttle experiment, *J. Phys. Oceanogr.*, 14, 242-254, 1984.

Yu, X., and M. J. McPhaden, Seasonal variability in the equatorial Pacific, *J. Phys. Oceanogr.*, 29, 925-947, 1999.

Y. Dandonneau, C. Dupouy, C. Menkes, and J. Vialard, LODyC, tour 15, 2ème étage, 4, place Jussieu, 75252 Paris cédex 05, France. (yd@lodyc.jussieu.fr; cdu@lodyc.jussieu.fr; cmlod@ipsl.jussieu.fr; jvlod@ipsl.jussieu.fr)

T. Delcroix, Centre IRD, BP A5, 98848 Nouméa cédex, New Caledonia. (delcroix@noumea.ird.nc)

P.-Y. Deschamps, LOA, Université des Sciences et Technologies de Lille, 59655 Villeneuve d'Ascq cédex, France. (Pierre-Yves.Deschamps@univ-lille1.fr)

C. Moulin and A. Stoens, LSCE, CE Saclay, Bât 709, 91191 Gif sur Yvette cédex, France. (moulin@lsce.saclay.cea.fr; stoens@lsce.saclay.cea.fr)

M.-H. Radenac, LEGOS, 14 avenue Édouard Belin, 31401 Toulouse cédex 4, France. (Marie-Helene.Radenac@cnes.fr)

(Received July 12, 2000; revised July 5, 2001;
accepted July 6, 2001.)